Oligodendrocyte degeneration and concomitant microglia activation directs peripheral immune cells into the forebrain

Uta Chrzanowski, Sudip Bhattarai, Miriam Scheld, Tim Clarner, Petra Fallier-Becker, Cordian Beyer, Sven Olaf Rohr, Christoph Schmitz, Tanja Hochstrasser, Felix Schweiger, Sandra Amor, Anja Horn-Bochtler, Bernd Denecke, Stella Nyamoya, Markus Kipp

Angaben zur Veröffentlichung / Publication details:

Chrzanowski, Uta, Sudip Bhattarai, Miriam Scheld, Tim Clarner, Petra Fallier-Becker, Cordian Beyer, Sven Olaf Rohr, et al. 2019. "Oligodendrocyte degeneration and concomitant microglia activation directs peripheral immune cells into the forebrain." *Neurochemistry International* 126: 139–53. https://doi.org/10.1016/j.neuint.2019.03.005.

Oligodendrocyte degeneration and concomitant microglia activation directs peripheral immune cells into the forebrain

Uta Chrzanowski[1], Sudip Bhattarai[1], Miriam Scheld[2], Tim Clarner[2], Petra Fallier-Becker[3], Cordian Beyer[2], Sven Olaf Rohr[1], Christoph Schmitz[1], Tanja Hochstrasser[1], Felix Schweiger[1], Sandra Amor[4,5], Anja Horn-Bochtler[6], Bernd Denecke[7], Stella Nyamoya[1] and Markus Kipp[8]

[1]Department of Anatomy II, Ludwig-Maximilians-University of Munich, 80336 Munich, Germany
[2]Institute of Neuroanatomy and JARA-BRAIN, Faculty of Medicine, RWTH Aachen University, 52074 Aachen, Germany
[3]Institute of Pathology and Neuropathology, University of Tuebingen, 72076 Tuebingen, Germany
[4]Department of Pathology, VU University Medical Centre, Amsterdam, The Netherlands
[5]Centre for Neuroscience and Trauma, The Blizard Institute Barts and The London, School of Medicine and Dentistry, Queen Mary University of London, London, UK
[6]Department of Anatomy I, Ludwig-Maximilians-University of Munich, 80336 Munich, Germany
[7]Interdisciplinary Center for Clinical Research, University Hospital RWTH Aachen, Aachen, Germany
[8]Institute of Anatomy, Medical University of Rostock, Rostock, Germany

Word counts: Introduction (647), Material and Methods (1751), Results (1807), Discussion (1487), Legends (1315), Bibliography (1637), Total (9252)
Number of figures: 7
Number of tables: 2

Corresponding author

Markus Kipp
Institut für Anatomie, Universitätsmedizin Rostock
Gertrudenstraße 9;18057 Rostock
mail: markus.kipp@med.uni-rostock.de
Phone: 0049 381 494 8401

Abstract

Brain-intrinsic degenerative cascades are a proposed factor driving inflammatory lesion formation in multiple sclerosis (MS) patients. We recently showed that encephalitogenic lymphocytes are recruited to the sites of active demyelination induced by cuprizone. Here, we investigated whether cuprizone-induced oligodendrocyte and myelin pathology is sufficient to trigger peripheral immune cell recruitment into the forebrain. We show that early cuprizone-induced white matter lesions display a striking similarity to early MS lesions, i.e., oligodendrocyte degeneration, microglia activation and absence of severe lymphocyte infiltration. Such early cuprizone lesions are sufficient to trigger peripheral immune cell recruitment secondary to subsequent EAE (experimental autoimmune encephalomyelitis) induction. The lesions are characterized by discontinuation of the perivascular glia limitans, focal axonal damage, and perivascular astrocyte pathology. Time course studies showed that the severity of cuprizone-induced lesions positively correlates with the extent of peripheral immune cell recruitment. Furthermore, results of genome-wide array analyses suggest that moesin is integral for early microglia activation in cuprizone and MS lesions. This study underpins the significance of brain-intrinsic degenerative cascades for immune cell recruitment and, in consequence, MS lesion formation.

Keywords: Moesin, multiple sclerosis, cuprizone, experimental autoimmune encephalomyelitis

Introduction

Multiple sclerosis (MS) is a neuroinflammatory disorder of the central nervous system (CNS), potentially leading to severe motor, sensory, or visual deficits. Clinically, MS represents one of the main causes of disability in the young adult, and thus has a high socio-economic impact. At the histopathological level, MS lesions are characterized by oligodendrocyte death, demyelination, gliosis, axonal damage, and peripheral immune cell infiltration (Bauer, Rauschka et al. 2001, Benn, Halfpenny et al. 2001). Despite decades of research, it is still not clear what causes the formation of new inflammatory lesions in MS patients.

MS can be, based on the disease course, clinically categorized into three groups: relapsing-remitting, secondary progressive, and primary progressive. In most patients, the initial course of the disease is relapsing-remitting which is characterized by acute clinical attacks that are followed by complete or incomplete recovery, and a period of remission in between the attacks. Many patients with an initial relapsing-remitting disease course develop secondary progressive MS. In these patients, a more or less continuous decline of neurological functioning occurs with or without occasional attacks (Lublin, Reingold et al. 2014). Primary progressive MS is characterized by the accumulation of clinical disability from the onset of symptoms, without early relapses or remissions.

It is broadly accepted that the histopathological correlate of acute attacks is a focal inflammatory demyelinating white matter lesion. These focal inflammatory lesions impact on neuronal integrity eventually leading to axonal dysfunction or complete axonal destruction (Ferguson, Matyszak et al.

1997, Kornek, Storch et al. 2000). Although the accumulation of peripheral immune cells is a characteristic of such lesions, it is not clear what triggers the influx of immune cells into the central nervous system (CNS). However, a degenerative process within the brain has been suggested as one potential trigger mechanism (De Groot, Bergers et al. 2001, Barnett and Prineas 2004, Scheld, Ruther et al. 2016, Ruther, Scheld et al. 2017). Indeed, that damage to the brain parenchyma can trigger the site of inflammatory lesion formation, is well known. In both - active immunization and passive transfer forms of experimental autoimmune encephalomyelitis (EAE) - an autoimmune animal model of MS, inflammatory lesions rapidly localize at sites of non-specific brain damage, including thermal brain injury (Levine and Hoenig 1968, Levine and Hoenig 1971), cyanide-induced encephalopathy (Levine 1960), cortical cryolesions (Phillips, Weller et al. 1995, Lake, Weller et al. 1999), experimental induction of Wallerian degeneration (Konno, Yamamoto et al. 1990), or cytokine injection (Sun, Newman et al. 2004). In humans, it has been suggested that mechanical stresses can determine the site of spinal cord MS lesions (Oppenheimer 1978). These studies clearly illustrate the significance of brain-intrinsic degenerative cascades for immune cell recruitment and MS lesion formation.

We recently demonstrated that cuprizone-induced demyelination can trigger peripheral immune cell recruitment into the forebrain after MOG_{35-55} immunization (Scheld, Ruther et al. 2016, Ruther, Scheld et al. 2017). In these studies, demyelination of the murine forebrains was induced by a 3-weeks cuprizone (Cup) intoxication protocol, followed by two weeks on normal chow. At week five, encephalitogenic T cells in peripheral lymphoid organs were generated by active immunization with the myelin oligodendrocyte glycoprotein 35–55 peptide ($MOG_{35–55}$) (Iglesias, Bauer et al. 2001). While peripheral immune cell recruitment was minimal in the forebrains of $MOG_{35–55}$-immunized mice (i.e., active EAE induction), cuprizone-induced demyelination revealed to be a potent trigger for the recruitment of monocytes, lymphocytes and granulocytes (Scheld, Ruther et al. 2016, Ruther, Scheld et al. 2017). A drawback of these previous studies using this so-called Cup/EAE model is, however, that active $MOG_{35–55}$ immunization was induced at a time when demyelination was already fully established. This is in contrast to proposed mechanisms operant during early MS lesion formation, i.e., oligodendrocyte degeneration and microglial activation associated with few lymphocytes and phagocytes in regions of relative myelin preservation (van der Valk and De Groot 2000, De Groot, Bergers et al. 2001, Barnett and Prineas 2004, Marik, Felts et al. 2007).

The purpose of this study was, therefore, to investigate whether a short-term cuprizone intoxication protocol is sufficient to trigger peripheral immune cell recruitment after MOG_{35-55} immunization. Additionally, by using gene array technology, we aimed at identifying factors orchestrating immune cell recruitment into the forebrains of Cup/EAE mice. We can show that cuprizone-induced oligodendrocyte degeneration with concomitant microglia activation is sufficient to trigger the recruitment of peripheral immune cells into the forebrain. Of note, the extent of cuprizone-induced tissue injury positively correlates with the number of focal inflammatory lesions after MOG_{35-55} immunization. Results of gene

array analyses and immunohistochemical stains suggest an important role of moesin^{+} microglia for the formation of the inflammatory foci.

Materials and Methods

Animals and experimental groups

8 week-old C57BL/6 female mice (19 g - 20 g) were purchased from Janvier Labs (Le Genest-Saint-Isle, France). Microbiological monitoring was performed according to the Federation of European Laboratory Animal Science Associations recommendations. A maximum of five animals were housed per cage (cage area 435 cm^2). Animals were kept under standard laboratory conditions (13 h light/11 h dark cycle, controlled temperature 22 °C ± 2 °C and 50 % ± 10 % humidity) with access to food and water *ad libitum*. It was assured that researchers and technicians did not use any light during the night cycle period. Nestlets were used for environmental enrichment. All experiments were formally approved by the Regierung Oberbayern (reference number 55.2-154-2532-73-15). Mice were randomly assigned to the following groups (see ***figure 3A***): (A) control, animals received a diet of standard rodent chow for the duration of the study; (B) 1wk cuprizone (Cup) /EAE, animals were fed a diet containing 0.25% cuprizone (bis(cyclohexanone)oxaldihydrazone; Sigma-Aldrich, Taufkirchen, Germany) mixed into ground standard rodent chow for one week, followed by normal chow for 24 h, and were then immunized with $MOG_{35–55}$ (Hooke Laboratories, Inc., Lawrence, USA) at the beginning of week two; (C) 3wks cup/EAE, animals were fed the cuprizone diet for three weeks, and were then immunized with $MOG_{35–55}$ at the beginning of week four; (D) 3 cup+2wks normal chow/EAE, mice were fed the cuprizone diet for the first three weeks and were then immunized with $MOG_{35–55}$ at the beginning of week six. Additional animals were fed the cuprizone diet for either 1wk, 3wks, or 5wks and 3 wks+2wks normal chow without any additional MOG_{35-55} immunization (not shown in ***figure 3A***). This experimental setup was published previously (Scheld, Ruther et al. 2016, Ruther, Scheld et al. 2017).

Multiple sclerosis tissues

Paraffin-embedded postmortem brain tissues were obtained through a rapid autopsy protocol from subjects with mainly progressive MS (in collaboration with the Netherlands Brain Bank, Amsterdam). The study was approved by the institutional ethics review board, and all donors or their relatives provided written consent for the use of brain tissues and clinical information for research purposes. Staging of lesions was performed as reported previously (van der Valk and De Groot 2000, Grosse-Veldmann, Becker et al. 2016, Trepanier, Hildebrand et al. 2018). In brief, active lesions are defined as hypercellular throughout the entire lesion, chronic active lesions are defined as a lesion with a hypocellular center and a hypercellular rim, and chronic inactive lesions are defined as hypocellular throughout the entire lesion. For the study, three chronic active and three chronic inactive lesions were included. The average age of patients in years was 56.8± 14.36 (mean ± SD). The average postmortem

delay in hours was 10.02 ± 0.3365. Staging of the white matter lesion activity was performed using anti-PLP and anti-MHC class II (LN3)-stained sections.

EAE and disease scoring

To induce the formation of encephalitogenic T cells in peripheral lymphatic tissues, mice were subcutaneously immunized with an emulsion of $MOG_{35–55}$ peptide dissolved in complete Freund's adjuvant followed by intraperitoneal injections of pertussis toxin in PBS (PTX) on the day of and the day after immunization (Hooke Laboratories, Inc., Lawrence, USA) as published previously (Ruther, Scheld et al. 2017). Disease severity was scored as follows: 1, the entire tail drops over the observer's finger when the mouse is picked up by base of the tail; 2, the legs are not spread apart but held close together when the mouse is picked up by base of the tail, and mice exhibit a clearly apparent wobbly gait; 3, the tail is limp and mice show complete paralysis of hind legs (a score of 3.5 is given if the mouse is unable to raise itself when placed on its side); 4, the tail is limp and mice show complete hind leg and partial front leg paralysis, and the mouse is minimally moving around the cage but appears alert and feeding (a score of 4 was not attained by any of the mice in our study).

Tissue preparation

For histological and immunohistochemical studies, mice were anaesthetized with ketamine (100 $mg \cdot kg^{-1}$ i.p.) and xylazine (10 $mg \cdot kg^{-1}$ i.p.), and transcardially perfused with ice-cold PBS followed by a 3.7% formaldehyde solution (pH 7.4). Brains were postfixed overnight in a 3.7% formaldehyde solution, dissected, embedded in paraffin, and then coronal sections (5 µm) were prepared (Acs, Kipp et al. 2009, Clarner, Diederichs et al. 2012). Spinal cords were incubated in a Na/EDTA (ethylenediaminetetraacetic acid) solution for 48 h (changed once after ~24h) at 37°C prior to paraffin embedding. For gene expression studies, tissues were manually dissected after transcardial PBS perfusion, immediately frozen in liquid nitrogen, and kept at -80°C until further processing.

Immunohistochemistry/Histochemistry and Evaluation

For immunohistochemistry, sections were rehydrated and, if necessary, antigens were unmasked by heating in Tris/EDTA (pH 9.0) or citrate (pH 6.0) buffer. After washing in PBS, sections were blocked in blocking solution (serum of the species in which the secondary antibody was produced) for 1 h. Then, sections were incubated overnight (4 °C) with primary antibodies diluted in blocking solution. The next day, slides were incubated in 0.3% hydrogen peroxide/PBS for 1 h and then incubated with biotinylated secondary antibodies for 1 h followed by peroxidase-coupled avidin-biotin complex (ABC kit; Vector Laboratories, Peterborough, UK). Sections were finally exposed to 3,3′-diaminobenzidine (DAKO, Santa Clara, CA, USA) as a peroxidase substrate as published previously (Hoflich, Beyer et al. 2016). To visualize cell nuclei, sections were stained with hematoxylin solution. Negative control sections without primary antibodies or with isotype antibodies were processed to ensure specificity of the

staining. Antibodies used in this study are listed in ***supplementary table 1***. Luxol fast blue (LFB)/periodic acid-Schiff (PAS) stains were performed following standard protocols.

Stained and processed sections were digitalized using a Nikon ECLIPSE 50i microscope (Nikon, Nikon Instruments, Düsseldorf, Germany) equipped with a DS-2Mv camera. The open source program ImageJ (NIH, Bethesda, MD, USA) was used to determine staining intensities, cellular densities and to quantify the densities of APP^+ spheroids at specified distances from inflamed vessels (0-100 µm). To evaluate staining intensity using semi-automated densitometrical evaluation after threshold-setting, acquired images were converted to grey scale images, and a global thresholding algorithm was used for dividing each image into two classes of pixels (black and white; i.e., binary conversion). Global thresholding works by choosing a value cutoff, such that every pixel less than that value is considered one class, while every pixel greater than that value is considered the other class. Relative staining intensity was then quantified in binary converted images, and results are presented as percentage area. To quantify the numbers and localization of perivascular cuffs (PVCs) per section in the forebrain, lesions were identified in hematoxylin and eosin (H&E)-stained sections by one evaluator blinded to the treatment groups, and the results were averaged per brain section. Forebrains were analyzed between the levels R215 and R295 according to the mouse brain atlas by Sidman et al. (http://www.hms.harvard.edu/research /brain/atlas.html) as published previously (Ruther, Scheld et al. 2017). For the analysis of $IBA1^+$ and $CD3^+$ cell densities in mice brains, and $moesin^+$ cell densities in human MS lesions, stained sections were scanned with the Zeiss Mirax Midi scanner (Zeiss, Carl Zeiss MicroImaging GmbH, Jena, Germany) equipped with a Stingray camera, and analyzed with the open source program ViewPoint Online (PreciPoint, Freising, Germany).

Immunofluorescence labeling

For immunofluorescence labelling, sections were deparaffinized, rehydrated, unmasked, and blocked in serum of the species in which the secondary antibody was raised. Sections were incubated overnight (4 °C) with the indicated combination of primary antibodies diluted in blocking solution. For double-labelling experiments, anti-moesin antibodies were either combined with goat anti-IBA1 for the detection of murine microglia, or anti-MHC-II (LN3) for the detection of activated microglia and monocytes in human tissues. Acute axonal injury was visualized with anti-amyloid precursor protein (APP) antibodies. After extensive washing, sections were incubated with a combination of fluorescent secondary antibodies. Sections were then incubated with Hoechst 33258 (bisBenzimide H 33258 Sigma Aldrich, Steinheim, Germany; 1:10,000) diluted in PBS for the staining of cell nuclei. To exclude unspecific binding of the fluorescent secondary antibodies to primary antibodies, negative controls were performed by first incubating sections with the primary antibodies and subsequently incubating these sections with the "wrong" secondary antibodies. Unspecific secondary antibody binding was excluded by incubating sections with the fluorescent secondary antibodies alone. Stained and processed sections were documented using an Olympus BX41-Wi fluorescence microscope station (Olympus, Germany).

Transmission electron microscopy

For ultrastructural studies, tissue samples were fixed in 2.5% glutaraldehyde (Science Services, Munich, Germany) cacodylate buffer (pH 7.4; Merck-Millipore, Darmstadt, Germany) at 4 °C overnight as described previously (Noell, Wolburg-Buchholz et al. 2012). Thereafter, samples were embedded in Araldite (Serva, Heidelberg, Germany), and ultrathin sections were cut using a Leica ultramicrotome (Leica, Wetzlar, Germany) and analyzed using a Zeiss EM-10 transmission electron microscope (Zeiss, Oberkochen, Germany).

Gene array analyses

Genome-wide gene expression of corpus callosum (CC) from control mice and mice fed with cuprizone (male) for 1 week was analyzed in independent quadruplicates using Affymetrix GeneChip® MouseGene1.0 ST Arrays. Total RNA was isolated using RNeasy Kits from QIAGEN, and quantity was assessed using the NanoDrop-1000 Spectrophotometer (Thermo Fisher Scientific, Wilmington, DE, U.S.A.) and RNA quality was assessed using the RNA 6000 NanoChips with the Agilent 2100 Bioanalyzer (Agilent, Waldbronn, Germany). Total RNA samples, each 150 ng, were prepared for the GeneChip® Mouse Gene 1.0 ST Arrays (Affymetrix, USA), and hybridized to the arrays according to the Ambion whole transcript expression and the Affymetrix whole transcript terminal labelling and control kits manuals. Processed samples were hybridized to the GeneChip® Mouse Gene 1.0 ST Arrays at 45°C for 16h with 60rpms, washed and stained on a Fluidics Station 450 (program FS450_00007) and scanned on GeneChip® Scanner 3000 7G (both Affymetrix). Raw image data were analyzed with Affymetrix® Expressin ConsoleTM Software, gene expression intensities were normalized and summarized with robust multiarray average algorithm (Irizarry, Hobbs et al. 2003). To identify genes differentially expressed between cuprizone treated and control mice a comparison analysis using Affymetrix Transcriptome Analysis Console (TAC) 4.0 Software was performed. Gene expression was considered as changed if transcript levels between cuprizone treated and control groups were differential with a 1.5-fold change and a FDR p value of < 0.05. Gene ontology enrichment analysis was performed using the "*Enrichment analysis*" tool (http://www.geneontology.org). The following items were applied: 'GO biological process' for annotation data set, 'Fischer's exact" for test-type, and Bonferroni correction for multiple testing. A list of up- and down regulated genes is provided in ***supplementary table 2***. The microarray data have additionally been deposited in the Gene Expression Omnibus database #GSE119672.

Statistical analyses

Statistical analyses were performed using Prism 5 (GraphPad Software Inc., San Diego, CA, USA). All data are given as arithmetic means ± SEMs. A p value of <0.05 was considered to be statistically significant. Applied statistical tests are given in the respective figure legends. No outliers were excluded from the analyses. No sample size calculation was performed.

Results

Histopathological characteristics of initial demyelinating MS lesions are (i) stressed oligodendrocytes with apoptotic-like nuclear changes, (ii) activated microglia, dispersed between seemingly intact myelin, and (iii) few if any lymphocytes (Barnett and Prineas 2004, Marik, Felts et al. 2007, Haider, Fischer et al. 2011, Prineas and Parratt 2012). In a first step, we investigated histopathological characteristics of early cuprizone lesions. Numerous apoptotic oligodendrocytes (i.e., condensed and/or fragmented nuclei of cells in a chain-like formation in H&E-stained sections, see arrows in ***figure 1A***) were observed in the CC of animals treated with cuprizone for one week. Apoptotic cells were absent in control animals. In both the cortex and the CC, numerous $ATF3^+$ cells were observed in cuprizone-intoxicated but not control animals (***figure 1B***), showing activation of a stress response in oligodendrocytes (Goldberg, Daniel et al. 2013). Immunohistochemical stains for three distinct myelin proteins, namely proteolipid protein (PLP), myelin-associated glycoprotein (MAG), and 2',3'-cyclic nucleotide 3' phosphodiesterase (CNPase), as well as the histochemical stain Luxol Fast Blue/Periodic acid-Schiff (LFB/PAS) demonstrated the absence of demyelination at week 1 (***figures 1C-F***), but severe demyelination after a 5 weeks continuous cuprizone intoxication period. The presence of intact myelin was also evident on the ultrastructural level (***figure 1J***) and verified in anti-myelin protein stained sections by unbiased densitometrical analyses (***figure 1K***). While anti-myelin staining intensities were unchanged after 1 and 3 weeks continuous cuprizone-intoxication, severe anti-PLP, anti-MAG and anti-CNPase staining intensities were observed after 5 weeks continuous cuprizone-intoxication. Anti-ionized calcium-binding molecule 1 (IBA1) staining of control brain sections showed cells with a small cell body and thin, highly ramified cell processes, both characteristics of resting microglia. After 1 week cuprizone exposure, cell processes were swollen and less ramified whereas cell bodies showed hypertrophy, indicating an activated microglia phenotype (***figure 1G***). Furthermore, densities of anti-$IBA1^+$ cells were significantly higher after 1 week of cuprizone intoxication (control: 83.7±11.4 versus 319.6±52.6 cells/mm^2, $p \leq 0.05$). $CD3^+$ and $CD4^+$ lymphocytes were virtually absent in control (0.0±0.0 $CD3^+$ cells/mm^2; n=5) and 1 week (3.7±1.5 $CD3^+$ cells/mm^2; n= 5) cuprizone-intoxicated animals (***figures 1H/I***). In summary, the histopathological characteristics of the initial demyelinating lesions in MS are well reproduced in mice following a one week cuprizone intoxication protocol.

Next, we investigated whether the observed histopathological changes are sufficient to trigger peripheral immune cell recruitment into the forebrain after MOG_{35-55} immunization. To this end, a second cohort of animals was intoxicated with cuprizone for one week and subsequently immunized with MOG_{35-55} peptide (group B in ***figure 3A***). A previous study reported that cuprizone intoxication in mice halts T cell mediated autoimmunity (Mana, Fordham et al. 2009). We, thus investigated whether the severity of clinical symptoms in classical MOG_{35-55}-immunized EAE mice was comparable in animals with or without previous cuprizone intoxication. Consequently, clinical scores were daily recorded and compared to mice fed normal chow prior to active EAE induction. No significant differences were

observed for the EAE parameters disease onset (EAE, 12.2 ± 0.3742 *vs* 1wk Cup/EAE, 10.8 ± 0.4899 d after immunization; p = 0.06) and maximum disease score (EAE, 2.7 ± 0.4673 vs 1 wk Cup/EAE, 2.5 ± 0.4183; p = 0.76) (***figures 2 A***).

In a next step, we analyzed the forebrains of treated mice at distinct rostral-to-caudal levels for the presence and localization of PVCs, a hallmark of active MS lesions (Maggi, Macri et al. 2014). This analysis was performed at the level of the anterior commissure (i.e., R215-235), the ventral hippocampal commissure (i.e., R245-265) and the rostral hippocampus (i.e., R275-295), respectively. As shown in ***figures 2B/C***, PVCs were virtually absent in the forebrains of control mice. Some infiltrates were found in the forebrains of MOG_{35-55}-immunized animals, and these were located predominantly around the third ventricle. In contrast, the forebrains of 1wk Cup/EAE animals contained a significant number of PVCs. Such infiltrates were widespread within the forebrain, including the cortex, CC, and subcortical regions.

Next, we examined whether the severity of cuprizone-induced injury (i.e., oligodendrocyte degeneration and microglia activation) correlates with the extent of peripheral immune cell recruitment. To investigate this aspect, two separate cohorts of animals were treated cuprizone for one or three weeks. A third cohort of animals was treated cuprizone for three weeks, followed by two weeks on normal chow (i.e., 3 weeks cuprizone + 2 weeks normal chow; 3+2) as published previously (see figure 3A) (Scheld, Ruther et al. 2016, Ruther, Scheld et al. 2017). First, we investigated myelination and microglia activation before the MOG_{35-55} immunization (see arrows in ***figure 3A*** which illustrates the time point of this analysis). As shown in ***figure 3B***, demyelination (PLP and LFB/PAS) of the corpus callosum was absent in 1 week, moderate in 3 weeks, but severe in 3+2 weeks intoxicated animals, respectively. Concomitant to the extent of demyelination, microgliosis (IBA1) was moderate at 1 week, intermediate at week 3, and severe in 3+2 weeks intoxicated animals. Next, additional animals were immunized with MOG_{35-55} peptide after week 1, 3 or 3+2 cuprizone, and numbers of PVCs were quantified two weeks after the immunization with the MOG_{35-55} peptide. As demonstrated in ***figure 3C***, the greater the extent of cuprizone-induced metabolic injury, the higher the number of PVCs. Numbers of PVCs per brain section were low in 1 week cup/EAE, intermediate in 3 weeks cup/EAE, and high in 3+2 weeks normal chow/EAE mice.

The resultant inflammatory foci were subsequently characterized at the level of the anterior commissure (i.e., R215) in the 1wk Cup/EAE animals. As shown in ***figure 4***, these focal inflammatory infiltrates are characterized by perivascular immune cell accumulation (i.e., within an enlarged Virchow-Robin space; ***figures 4A/A';***H&E), perivascular microgliosis/infiltrating macrophages (***figures 4B/B';*** IBA1), and moderate demyelination (***figures 4C/C';*** LFB/PAS). Double staining experiments for CD3 (green) and GFAP (red) showed that lymphocytes progressed through the astrocytic *glia limitans perivascularis* to invade the surrounding neuropil (***figure 4D***; see arrowhead). Although anti-GFAP immunoreactivity principally increased around the lesions (***figure 4E***), the staining intensity was lost especially in

perivascular regions with high immune cell density (***figure 4F***). Similar observations were made, if astrocytes were visualized with anti-ALDH1L1 antibodies (data not shown). To examine the presence of acute axonal injury around inflammatory infiltrates, we identified lesions in H&E-stained slides and stained adjacent sections with anti-APP antibodies, a marker for acute axonal injury (Hoflich, Beyer et al. 2016). The density of APP^+ spheroids was assessed in concentric areas around the vessel centers. As shown in ***figures 4G/H***, spheroid densities were highest in the immediate vicinity of the vessel and progressively declined with increasing distance. In summary, our results demonstrate that in the applied animal model oligodendrocyte apoptosis with concomitant microglia activation is sufficient to trigger peripheral immune cell recruitment into the forebrain after MOG_{35-55} immunization.

We next aimed to identify the factors linked to peripheral immune cell recruitment in the cuprizone model. Total mRNA samples from the CC of control mice and mice intoxicated with cuprizone for 1 week were analyzed using Affymetrix GeneChip® arrays. When a threshold of 1.5-fold regulation (control *versus* cuprizone) was applied, the expression of 344 probe sets was significantly up-regulated, whereas the expression of 227 probe sets genes was significantly reduced. As shown in ***figures 5A/B***, 2D principal components analysis (PCA) clearly revealed similarities between the individual samples (i.e., the formation of clusters), demonstrating the reliability of the experiment. For a better interpretation of our gene expression data, ***figure 5C*** shows a heatmap (each column: one individual animal), where red represents up-regulated genes and blue represents down-regulated genes in cuprizone-intoxicated *versus* control animals. Black represents unchanged gene expression levels. As demonstrated, the expression of well-known oligodendrocyte specific genes, such as *Mag* (myelin associated glycoprotein), *Mal* (myelin and lymphocyte protein), *Aspa* (aspartoacylase) or *Mog* (myelin oligodendrocyte glycoprotein) was significantly reduced after 1 week of cuprizone intoxication (lower-right cluster in ***figure 5C***). In contrast, the expression of chemokines which have been shown to be induced during the course of cuprizone-induced demyelination, such as *Cxcl0* (Clarner, Janssen et al. 2015) or *Ccl3* (Janssen, Rickert et al. 2016) showed higher expression levels (upper-right cluster). For a complete list of up- and down-regulated genes see ***supplementary table 2***. Next, we performed a gene ontology enrichment analysis with the detected down- and up-regulated genes, respectively. Computing genes for which expression was found to be down-regulated revealed greatest enrichments for the biological process terms 'central nervous system myelination' (28.5-fold enrichment), 'cholesterol biosynthetic process' (20.5-fold enrichment), 'Schwann cell differentiation' (16.2-fold enrichment), and 'regulation of gliogenesis' (7.5-fold regulation). Computing genes for which expression was found to be up-regulated revealed greatest enrichments for the biological process terms 'antigen processing and presentation of exogenous peptide antigen via MHC class I' (51.9-fold enrichment), 'positive regulation of tumor necrosis factor biosynthetic process' (29.9-fold enrichment), 'MyD88-dependent toll-like receptor signaling pathway' (24.3-fold enrichment), and 'response to interferon-alpha' (22.7-fold regulation). This result further supports our hypothesis that cuprizone-induced oligodendrocyte injury

activates pathways which are involved in the local (re-) activation of peripheral immune cells (see ***supplementary table 2*** for a complete list of genes and expression values).

One of the genes which displayed high expression induction was moesin (*Msn*). This protein belongs to the ezrin-radixin-moesin (ERM) family of proteins, which plays structural and regulatory roles in the rearrangement of plasma membrane flexibility and protrusions through interaction with cortical actin filaments and the plasma membrane (Pore and Gupta 2015). Since it has been reported that moesin is expressed in microglia/macrophages (Moon, Kim et al. 2011, Kashimoto, Yamanaka et al. 2013), and microglia activation is one characteristic feature of early cuprizone lesions, we focused on this particular ERM-protein.

To verify our gene array data, and to visualize which cell type(s) express moesin, brain slides from control and 1 week cuprizone-intoxicated mice were processed for immunohistochemistry. As shown in ***figures 6A-C***, low densities of moesin$^+$ cells were found in the CC and cortex of control animals. Moesin$^+$ cells showed morphological characteristics of either endothelial cells (Berryman, Franck et al. 1993) (arrow in ***figure 6B'*** and insert which shows a CD34/moesin double-stain) or microglia (arrow in ***figure 6C'***). Densities of moesin$^+$ cells were higher in both brain regions after 1 week cuprizone intoxication (***figures 6D/E***). To verify that the non-endothelial, moesin$^+$ cell population belongs to the microglia cell lineage, adjacent sections were processed for IBA1/moesin immunofluorescence double staining experiments. As demonstrated in ***figures 6 F/G***, there was a clear co-localization of the anti-moesin and anti-IBA1 signal. Blinded evaluation revealed that virtually all moesin$^+$ cells co-express IBA1 (data not shown). Furthermore, CD3/moesin immunofluorescence double staining experiments showed that lymphocytes expressed moesin as well (***figure 6H***).

Finally, we analyzed moesin expression in the brains of MS patients. In normal appearing grey matter tissues (i.e., no evidence of demyelination), moesin was prominently localized to structures what appeared to be endothelial cells (arrowhead in ***figures 7A/B***). Occasionally glial cells, possibly microglia, were moesin immunoreactive (see arrow in ***figure 7B***). No apparent immunoreactivity was detected in what appeared to be neurons. Comparable to what we found in the cortex, structures what appeared to be endothelial cells and microglia cells were moesin$^+$ in the normal appearing white matter (NAWM). Of note, the used antibody recognized the fine processes of scattered microglia (see arrow in ***figure 7C***). Next, we analyzed moesin expression in six different MS lesions (i.e., three chronic active and three chronic inactive lesions). A representative chronic active lesion is shown in ***figures 7D-F and H***. On the histopathological level, this lesion is characterized by focal demyelination (***figures 7D/E***), and accumulation of MHC-II$^+$ microglia/monocytes particularly at the rim of the lesion (***figure 7F/G***). A high density of moesin$^+$ cells was observed at the rim of chronic active MS lesions (***figure 7I***). Furthermore, as shown in ***figure 7J***, moesin$^+$ cells were observed in enlarged perivascular spaces, indicating that peripheral immune cells express moesin in MS as well. Slightly reduced densities of moesin$^+$ cells were found in the NAWM (***figure 7K***) and inactive lesion areas such as the center of

chronic inactive lesions (***figure 7L)***. Blinded quantification of moesin$^+$ cells in three chronic active lesions revealed lowest densities in the NAWM, and highest densities within the active lesion areas (***figure 7N; p=0.1042)***. MHC-II/moesin immunofluorescence double staining experiments (***figure 7M***) verified that virtually all MHC-II$^+$ cells express moesin. However, not all moesin$^+$ cells were MHC-II$^+$ (~88%), suggesting that moesin stains both activated and non-activated microglia/macrophages and endothelial cells.

Discussion

Here, we describe that early cuprizone lesions, which are characterized by oligodendrocyte apoptosis and microglia activation, trigger peripheral immune cell recruitment into the forebrain after MOG_{35-55} immunization. On the one hand, this study clearly illustrates the significance of brain-intrinsic degenerative cascades for immune cell recruitment and, possibly, MS lesion formation. On the other hand, our findings add to the understanding of the Cup/EAE model, a practical and effective tool for studying immune cell recruitment into the forebrain. Of note, the model has great translational potential, as most imaging and pathological MS studies are performed in the forebrain. By contrast, most EAE studies focus on spinal cord tissues.

Pathological changes associated with the formation of new inflammatory MS lesions are difficult to study, because such lesions are rarely fatal. Two main strategies can be pursued to understand underlying mechanisms of MS lesion formation: (i) To describe pathological findings in patients who died relatively early after the onset of a new symptomatic lesion, or (ii) to investigate brain biopsies of patients diagnosed with tumefactive MS, also called “pseudotumoral MS”, a well-recognized variant of MS (Hardy, Tobin et al. 2016, Totaro, Di Carmine et al. 2016). Following the first approach, Barnett and Prineas reported that the earliest pathological changes, described as prephagocytic lesions, consist of oligodendrocyte apoptosis and microglial activation associated with few lymphocytes and phagocytes in regions of relative myelin preservation. This was reported to be followed by the disappearance of oligodendrocytes and the presence of intramyelinic edema with tissue vacuolization. Finally, the myelin sheaths were fragmented and phagocytosed by macrophages in the presence of infiltrating T cells (Barnett and Prineas 2004). The earliest steps during the evolution of new, inflammatory lesions was, therefore, oligodendrocyte stress, paralleled by microglia activation. Similar observations were reported by others. For example, De Groot and colleagues subjected unfixed post-mortem brain slices to T(1)- and T(2)-weighted magnetic resonance imaging, followed by macroscopic and microscopic examination of the tissues. The authors described so-called ‘preactive’ lesions and speculated that this lesion type might represent one of the earliest stages during MS lesion development (De Groot, Bergers et al. 2001). Preactive lesions were observed throughout the normal-appearing white matter and were characterized by clustering of activated microglia in the absence of overt demyelination (van der Valk and De Groot

2000). The presence of stressed oligodendrocytes in these preactive lesions was reported later (van Noort, Bsibsi et al. 2010) while van Horssen et al (2012) showed that the pre-active lesions were not associated with blood-brain barrier disruption, suggesting that an intrinsic trigger of innate immune activation, rather than extrinsic factors crossing a damaged blood-brain barrier, induces the formation of clusters of activated microglia (van Horssen, Singh et al. 2012). In another study, Marik and colleagues found abundant areas of microglial activation in the absence of detectable demyelination in human MS autopsy tissues. Such areas of microglial activation were localized in a broad zone surrounding the border of actively demyelinating lesions, and less frequently also presented as separate lesions, which occurred independently from actively demyelinating plaques (Marik, Felts et al. 2007). Of note, such 'pre-demyelinating' lesions were specific for pattern III demyelination, in which oligodendrocyte apoptosis is a major characteristic (Lucchinetti, Bruck et al. 2000). The authors suggested that focal areas of microglial activation may precede the formation of demyelinating plaques in MS patients exhibiting hypoxia-like, pattern III demyelination. Comparably, Henderson and colleagues demonstrated that early loss of oligodendrocytes along with macrophage activation is a prominent feature in tissues bordering rapidly expanding MS lesions. Of note, parenchymal lymphocytes were largely absent in such areas (Henderson, Barnett et al. 2009). In another study using EAE in marmosets, Maggi and colleagues compared serial *in vivo* magnetic resonance imaging (MRI) to postmortem tissues. Here the authors show that early inflammatory lesions in EAE are characterized by focal microglia and astrocyte activation in the absence of demyelination and parenchymal lymphocytes (Maggi, Macri et al. 2014). Likewise, in MS, serial MRI studies have shown that focal changes in the normal appearing white matter are present at locations that later develop into focal T2 lesions that enhance with gadolinium (Filippi, Rocca et al. 1998, Narayana, Doyle et al. 1998). Such MRI studies have revealed that MS lesions are initiated several days or weeks before the appearance of the classical inflammatory demyelinating plaque (Filippi, Rocca et al. 1998, Narayana, Doyle et al. 1998) indicating that the blood-brain barrier appears to be intact at the earliest stages of lesion development.

Taken together, all these findings suggest a key role for brain intrinsic pathological processes during the earliest stages of MS lesion formation, and that areas of microglia activation precede the full-fledged inflammatory demyelination. Here, we demonstrate that several histopathological characteristics of early MS lesions are reproduced by a short-term cuprizone intoxication protocol, *id est* oligodendrocyte stress, focal microglia activation, absence of lymphocytes and absence of overt demyelination (see ***figure 1***). These findings are in line with previous reports (Buschmann, Berger et al. 2012, Hagemeier, Lurbke et al. 2013, Clarner, Janssen et al. 2015). In the present study, oligodendrocyte stress was detected by either the visualization of apoptotic bodies or the presence of $ATF3^{+}$ cells. Also not formally proven in the current study, we previously reported that activated caspase 3-expressing cells are found in close vicinity to CNPase-reactive fibers after short-term cuprizone intoxication (Buschmann, Berger et al. 2012), and that ATF3-expressing cells co-express the oligodendrocyte marker protein CC-1

(Goldberg, Daniel et al. 2013). The presence of apoptotic cells in the CC of cuprizone-intoxicated mice has been well reported by other groups (Acs and Komoly 2012, Hagemeier, Lurbke et al. 2013). Comparably, early microglia activation after short-term cuprizone intoxication has also been reported by us and other groups (Hagemeier, Lurbke et al. 2013, Clarner, Janssen et al. 2015, Krauspe, Dreher et al. 2015). Our studies thus support the finding that early cuprizone lesions are characterized by oligodendrocyte stress which leads to oligodendrocyte degeneration and concomitant microglia activation. Of note, whether minor demyelination is present in such early lesions remains to be clarified in future studies.

How this relatively mild pathological process triggers peripheral immune cell recruitment is currently unclear. Early studies in the sixties showed that many focal CNS injuries can principally trigger the formation of EAE lesions in these damaged areas. This has been shown for electrical or thermal burns (Clark and Bogdanove 1955, Bogdanove and Clark 1957, Levine and Hoenig 1968), implantation of chemicals (Levine, Zimmerman et al. 1963), or anoxic injuries (Levine and Wenk 1967). The gene array analyses conducted in this study revealed that cuprizone-induced oligodendrocyte apoptosis is paralleled by expression induction of genes known to regulate the cytoskeletal network. One of these induced proteins is moesin. Moesin, a **m**embrane-**o**rganizing **e**xtension **s**pike prote**in**, belongs to the ezrin/radixin/moesin family of proteins distributed in the plasma membrane in the cellular cortex. Collectively, these three proteins are also known as the ERM protein family. Under physiological conditions, microglial cells exhibit a highly ramified morphology characterized by motile processes that constantly monitor their immediate surrounding by extending and retracting their processes (Nimmerjahn, Kirchhoff et al. 2005). In case of a harmful event, the generation of effective immune responses by microglia necessitates their morphological transformation (or "activation"). During activation microglia cells retract their processes, and their cell bodies become hypertrophic. The ERM family proteins are in this context of particular interest as they orchestrate the assembly and stabilization of plasma membrane interactions through their ability to interact with transmembrane proteins and the cytoskeleton (Fehon, McClatchey et al. 2010). In doing so, they provide structural links to strengthen the cell cortex and facilitate several key cellular process, including the membrane dynamics, substrate adhesion, cell survival, determination of cell shape, polarity, formation of membrane protrusions, cell adhesion and motility (Pore and Gupta 2015, Pines, Levi et al. 2017). In this study, we demonstrated that induction of moesin expression is a robust and early event in the cuprizone model. Immunofluorescence double labelling experiments showed that besides endothelial cells, moesin is expressed by $IBA1^+$ microglia. Furthermore, activated, $LN3^+$ microglia/monocytes express moesin in MS lesions. It has been shown that moesin is expressed by, and functionally active in endothelial cells (Berryman, Franck et al. 1993, Schwartz-Albiez, Merling et al. 1995, Vitorino, Yeung et al. 2015). Expression and/or activation of moesin in microglia is less well appreciated, but microglia in the spinal cord were found to express moesin in a model of peripheral nerve injury (Kashimoto, Yamanaka et al. 2013). Furthermore, it has been shown that microglia express moesin in cryogenic traumatic brain injury

of the mouse cortex (Moon, Kim et al. 2011). In the latter study, moesin expression was also observed in resting microglia (Moon, Kim et al. 2011). In MS lesions we frequently found round, small moesin-expressing cells, reminiscent of lymphocytes and moesin$^+$ cells within the enlarged perivascular spaces of MS lesions (see ***figures 7I***). At least in mice we can show that moesin expression is not restricted to monocytes, but can also be expressed by T cells (Schwartz-Albiez, Merling et al. 1995, Ansa-Addo, Zhang et al. 2017). Of note, it has recently been shown that moesin controls differentiation of regulatory T cells (Ansa-Addo, Zhang et al. 2017) and regulates lymphocyte trafficking (Nomachi, Yoshinaga et al. 2013). To our knowledge, this is the first report, demonstrating expression of moesin in MS lesions, however the function of moesin during lesion formation and progression is currently not known. Moesin knock-down animals develop normally and are fertile, with no obvious histological abnormalities in any of the tissues examined. Whether moesin deficient mice develop less severe demyelination in the cuprizone model, and whether these mice are protected from active EAE are unknown and may provide important information for lesion formation in MS.

As mentioned in the results section of this manuscript, the mRNA expression of well-known oligodendrocyte specific genes was significantly reduced after 1 week of cuprizone intoxication. However, we did not find any evidence of demyelination at week 1 on the histochemical and immunohistochemical level (see ***figure 1***). In a recent paper we were able to demonstrate that cuprizone-induced oligodendrocyte apoptosis is paralleled by the activation of the endoplasmic-reticulum stress response (Fischbach, Nedelcu et al. 2018). One component of the endoplasmic-reticulum stress response is the selective and regulated degradation of mRNA, termed regulated IRE1-dependent decay (RIDD), which relieves endoplasmic-reticulum stress by reducing the amount of the endoplasmic-reticulum protein load. We speculate that although myelin protein synthesis is reduced in the stressed oligodendrocytes, the myelin sheaths remain stable for several days or even weeks before demyelination is visible on the histological level.

In summary, this study indicates that oligodendrocyte degeneration and concomitant microglia activation might trigger peripheral immune cell recruitment in MS, and thus, the formation of focal inflammatory lesions. A better understanding of the underlying mechanisms would allow approaches to suppress the development of inflammatory MS lesions at their earliest stages.

Conflict of interest: The authors declare no competing financial interests.

Acknowledgements: This study was supported by the Dr. Robert Pfleger Stiftung (M.K.) and the Deutsche Forschungsgemeinschaft (KI 1469/8-1). The technical support from P. Ibold, H. Helten, S. Wübbel, B. Aschauer, and A. Baltruschat is acknowledged.

Figures

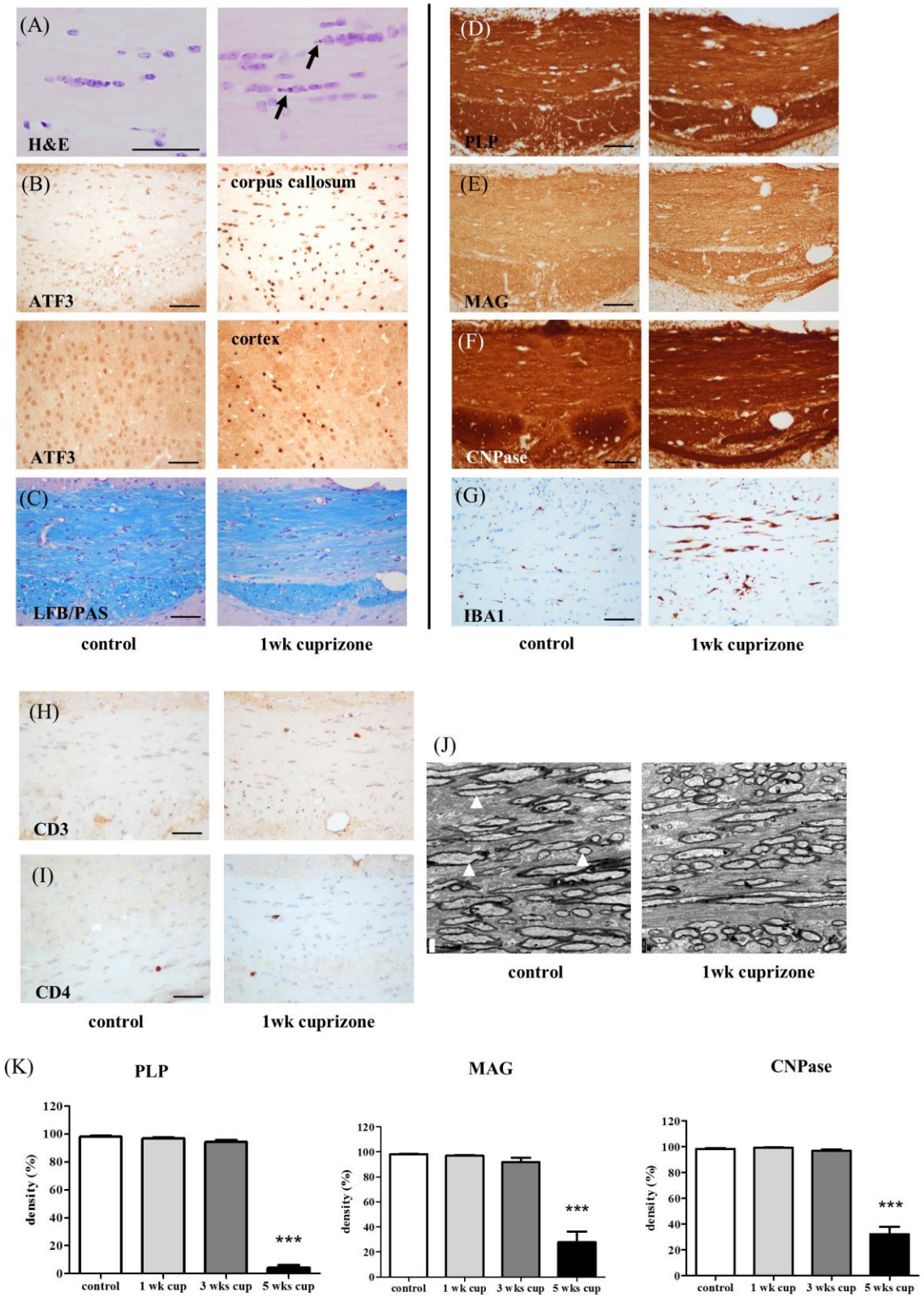

Figure 1: Histopathological characteristics of the 1 week cuprizone lesion

(A) Representative H&E-staining to visualize apoptotic cells (arrows). (B) Anti-activating transcription factor 3 (ATF3) expression in the corpus callosum (CC) (upper row) and cortex (lower row) to

demonstrate stressed oligodendrocytes. (C) Luxol fast blue (LFB)/periodic acid-Schiff (PAS) stain, (D) anti-proteolipid protein (myelin) 1 (PLP), (E) anti-myelin-associated glycoprotein (MAG) and (F) anti-2',3'-cyclic nucleotide 3' phosphodiesterase (CNPase) stain to demonstrate the myelination status of the corpus callosum. (G) Anti- ionized calcium-binding adapter molecule (IBA1) stain to demonstrate microglia activation. (H) Anti-CD3 and (I) anti-CD4 stain to demonstrate absence of T-lymphocytes in the CC. (J) Representative electron-microscopy images to demonstrate intact myelination on the ultrastructural level. Arrowheads indicate myelinated axons. (K) Quantification of anti-myelin proteins densities (i.e., anti-PLP, anti-MAG and anti-CNPase) of control, 1 week (wk), 3 wks, and 5 wks cuprizone (cup) animals (n=4-5 per group). Statistical comparison was done using a one-way ANOVA with the obtained p-values corrected for multiple testing using the Dunnett's post hoc test. Significant differences with respect to the control animals are indicated by *** $p<0.001$.
(A) Scale bar: 25 µm. (B-I) Scale bar: 50µm. (J) Scale bar: 1000 nm.

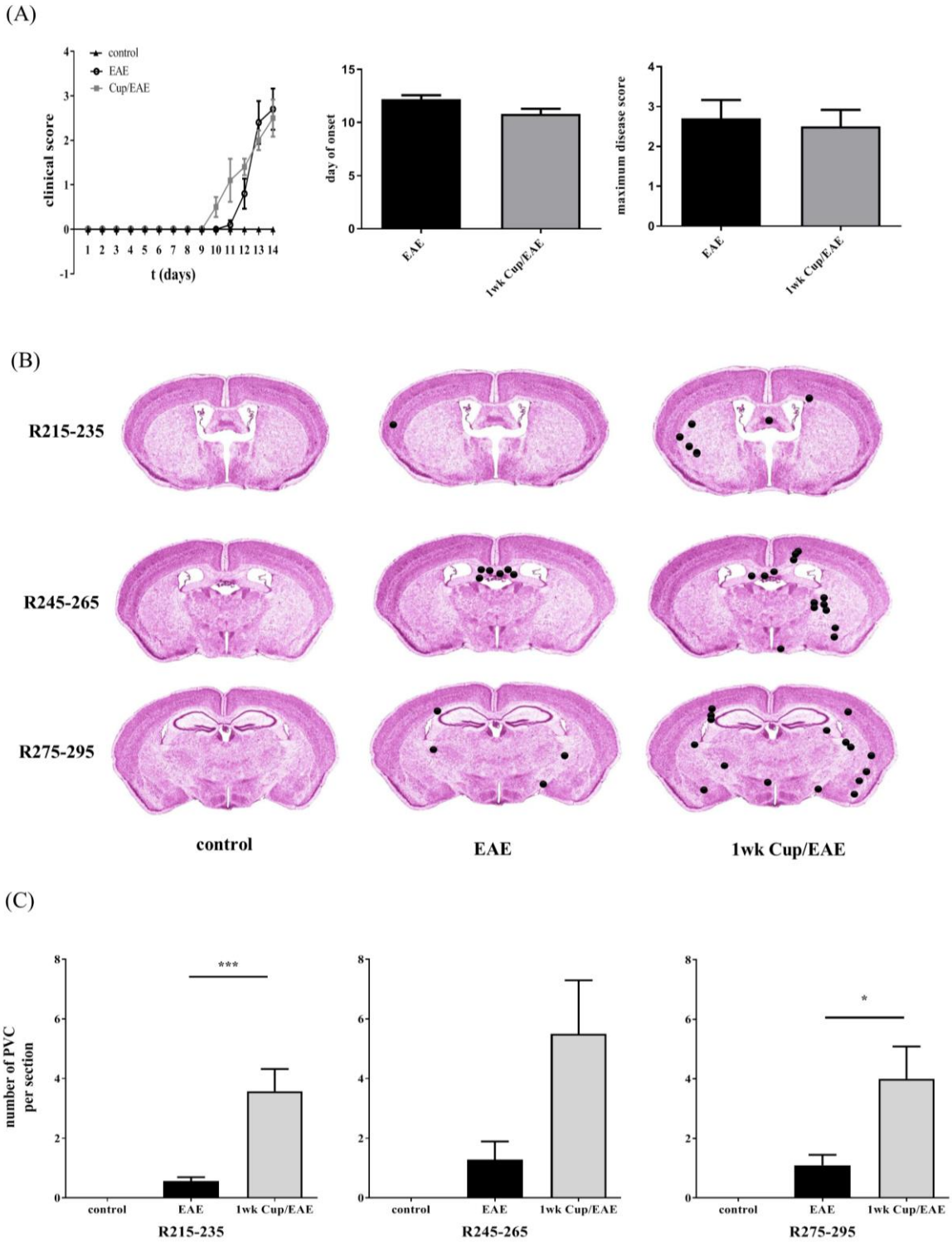

555

556 *Figure 2: Clinical disease progression and forebrain inflammatory cell infiltration*

557 (A) Clinical scores of control, experimental autoimmune encephalomyelitis (EAE) and 1wk cuprizone/

558 EAE (1wk Cup/EAE) mice. Five animals per experimental group, one representative experiment. The

559 left image shows the progression of clinical disease in the three different cohorts of mice. The center

image shows the mean day of disease onset of EAE and 1wk Cup/EAE mice. The right image shows the mean maximum disease score of EAE and 1wk Cup/EAE mice. Comparison of the mean day of disease onset and maximum disease score were done using unpaired t-test. (B) Distribution of perivascular cuffs (PVCs) in the different treatment groups (H&E staining; black dots from one independent observer) at three brain levels (regions according to Sidman et al.). (C) Quantification of the number of PVCs at three distinct brain levels. At R215-235, 33 slides were analyzed in control animals (n=4), 44 slides in EAE animals (n=5), and 40 slides in 1wk Cup/EAE animals (n=5). At R245-265, 7 slides were analyzed in control animals (n=4), 7 slides in EAE animals (n=5), and 8 slides in 1wk Cup/EAE animals (n=5). At R275-295, 8 slides were analyzed in control animals (n=4), 10 slides in EAE animals (n=5), and 8 slides in 1wk Cup/EAE animals (n=5). Comparison of the numbers of PVCs was done using one-way ANOVA with the obtained p-values corrected for multiple testing using the Tukey's post hoc test. Significant differences in between the three experimental groups are indicated by $*p < 0.05$, $**p < 0.01$, or $***p < 0.001$.

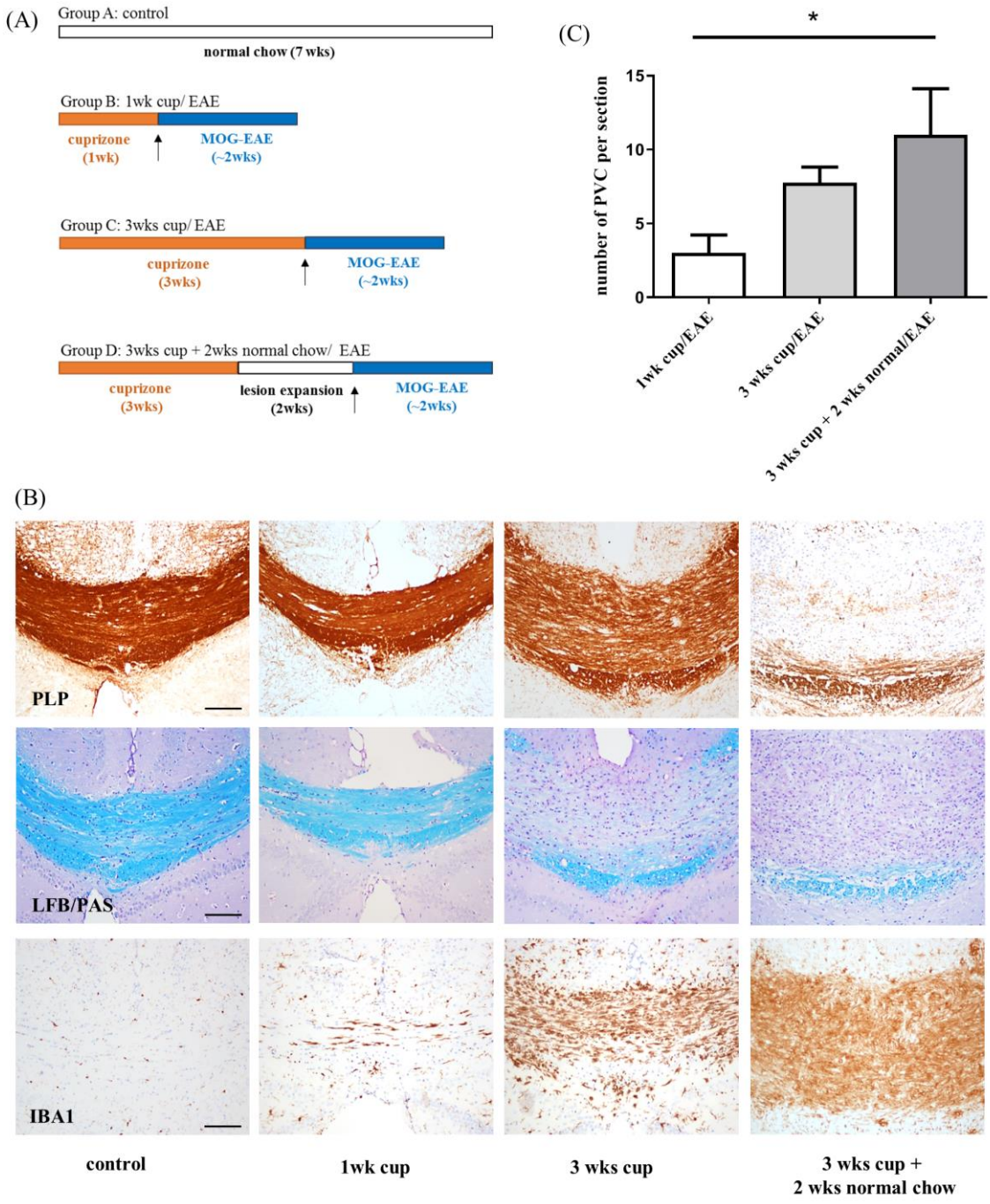

Figure 3: Correlation between severity of demyelination and forebrain inflammatory cell infiltration

(A) Schematic depicting the experimental setup. (B) Anti-proteolipid protein (myelin) 1 (PLP)-stain (upper-row), Luxol fast blue (LFB)/periodic acid-Schiff (PAS) stain (middle-row) and anti-ionized calcium-binding adapter molecule-stain (lower-row, IBA1) to demonstrate demyelination and concomitant microgliosis of the corpus callosum. Animals were subjected to a 1 week or 3 weeks continuous cuprizone intoxication protocol. One additional group was intoxicated with cuprizone for 3 weeks, followed by 2 weeks on normal chow before scarification. (C) Quantification of the number of perivascular cuffs (PVCs) per section at the level R215 in 1wk Cup/EAE (n=9), 3wks Cup/EAE (n=8) or 3 wks followed by 2 wks on normal chow/EAE (n=5) mice. Comparison of the numbers of PVCs per

583 section was done using one-way ANOVA with the obtained p-values corrected for multiple testing using
584 the Tukey's post hoc test. Significant differences in between the three experimental groups are indicated
585 by *p < 0.05.
586 (A) Scale bar: 100 µm.

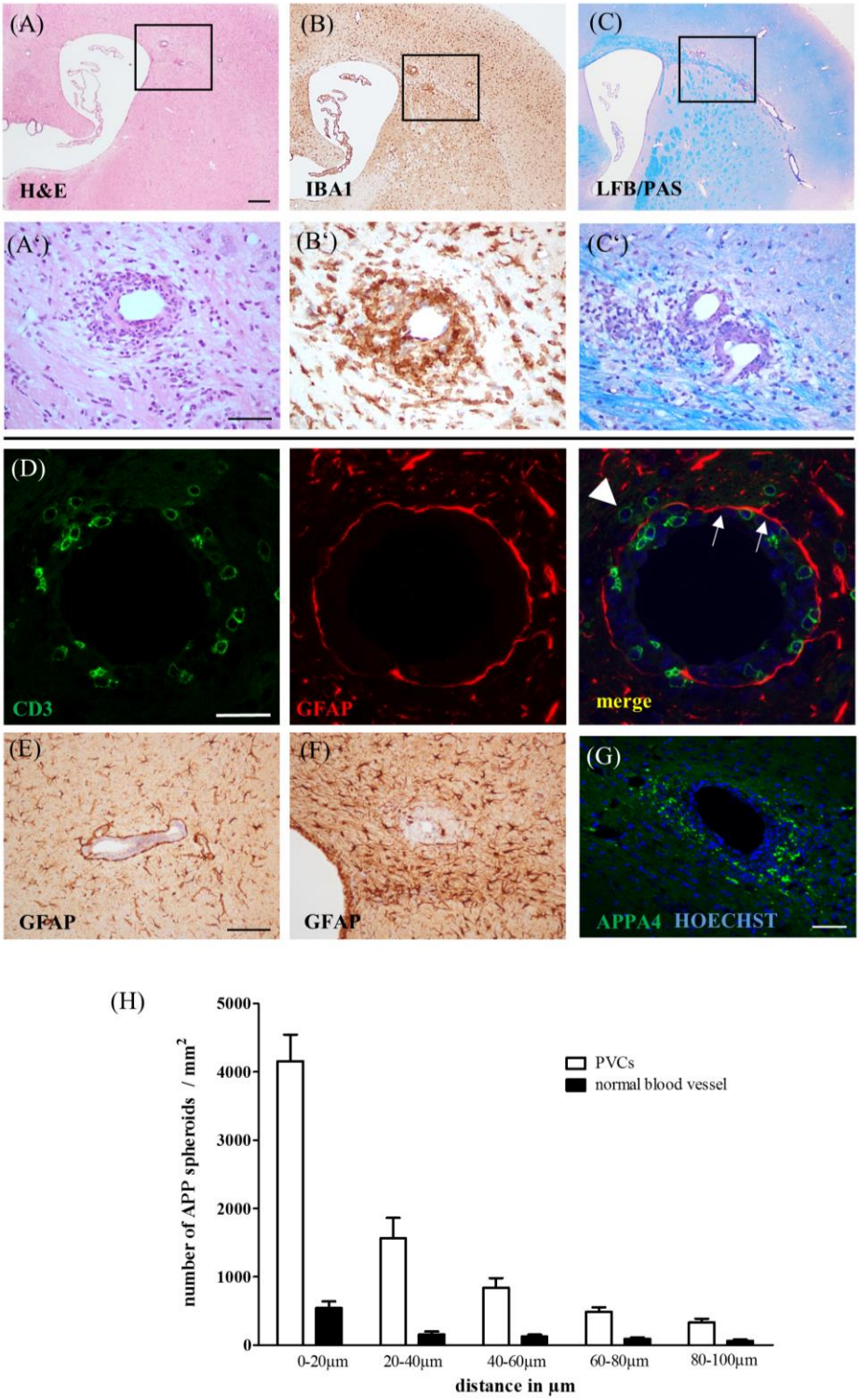

Figure 4: Forebrain inflammatory cell infiltration and acute axonal injury.

Representative perivascular cuffs (PVCs) of a 1wk Cup/EAE mouse at R225 (see figure 3 for grouping). (A/A') H&E staining to demonstrate a perivascular lesions in which most immune cells are trapped in the enlarged perivascular space. (B/B') Anti- ionized calcium-binding adapter molecule (IBA1) stain to demonstrate perivascular microglia and monocyte accumulation. (C/C') Luxol fast blue (LFB)/periodic acid-Schiff (PAS) stain to demonstrate partial demyelination around a perivascular lesion where

immune cells invaded the neuropil. (D) Anti- CD3 and anti-glial fibrillary acidic protein (GFAP) double stain to demonstrate migration of lymphocytes over the *glia limitans perivascularis* into the surrounding neuropil. Arrows indicate the *glia limitans perivascularis* whereas the arrowhead indicates a $CD3^+$ lymphocyte in the perivascular neuropil. (E/F) Anti-GFAP stain to demonstrate astrocyte pathology around PVCs. (G) Anti-amyloid beta (A4) precursor protein (APP) stain to demonstrate acute axonal injury in perivascular areas as spheroids. Counterstaining with Hoechst 33258 (blue) to show the cell nuclei. (H) APP^+ spheroid densities were quantified in concentric areas (up to 100 µm) from the vessel center. Inflamed (white columns) and normal vessels (black columns) were included. For each sector, 25 perivascular regions with and without lesions (5-6 animals) were analyzed.

(A-C) Scale bar: 250 µm. (A'-C', G) Scale bar: 50 µm. (D) Scale bar: 25µm. (E-F) Scale bar: 100µm

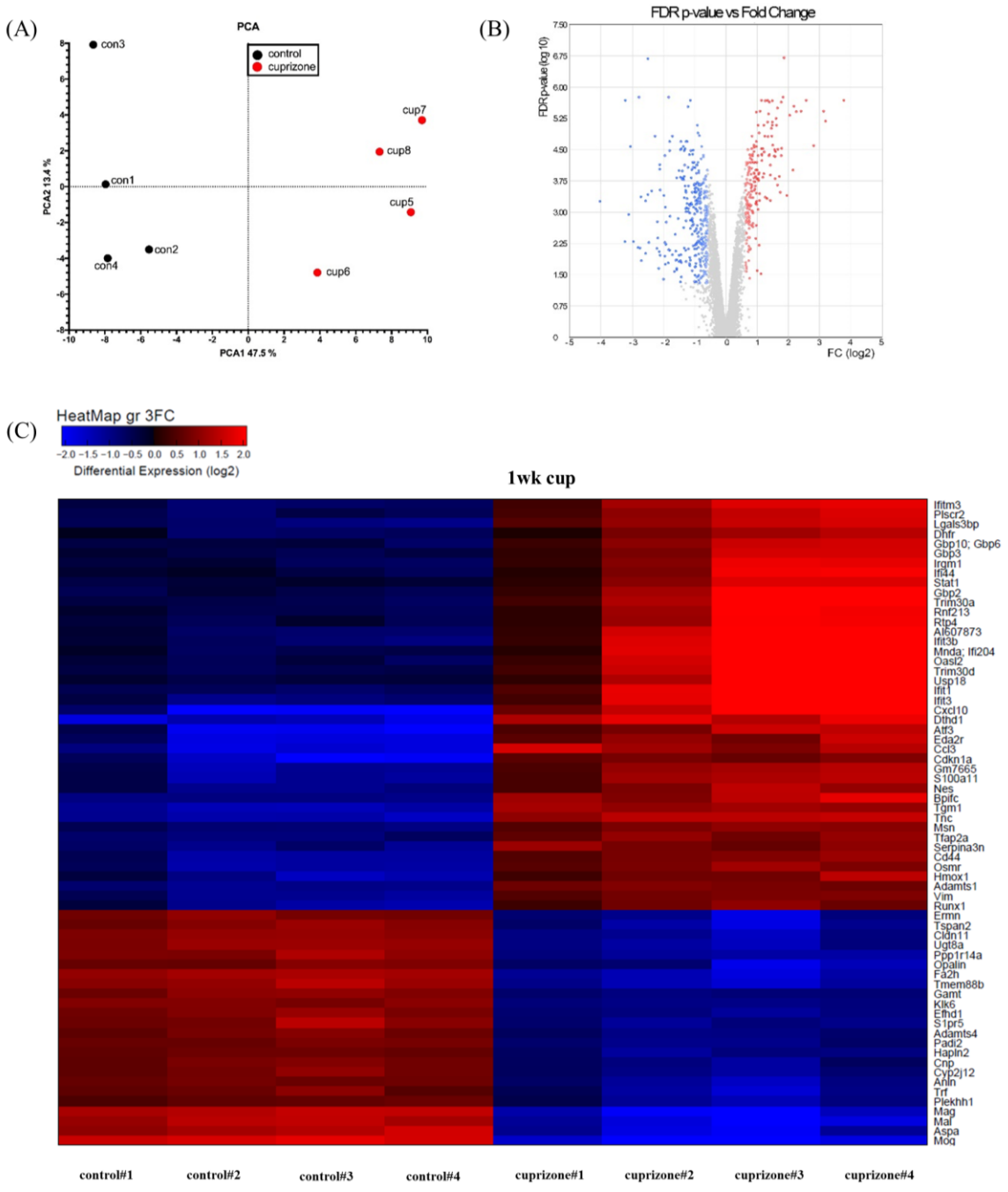

Figure 5

(A) Principal component 2D-analysis (PCA) of the gene expression data set. Each dot represents a corpus callosum sample. (B) Volcano plot of differentially abundant transcripts. (C) Heatmap in which genes have been grouped based on their pattern of gene expression. Each column represent one individual animal (control: 4 animals; 1 week cuprizone: 4 animals). The color and intensity of the boxes is used to represent changes (not absolute values) of gene expression. Red represents up-regulated genes and blue represents down-regulated genes. Black represents unchanged expression. Only genes significantly (FDR p-value < 0.05) differentially expressed with a minimal change in expression by 3-fold are illustrated.

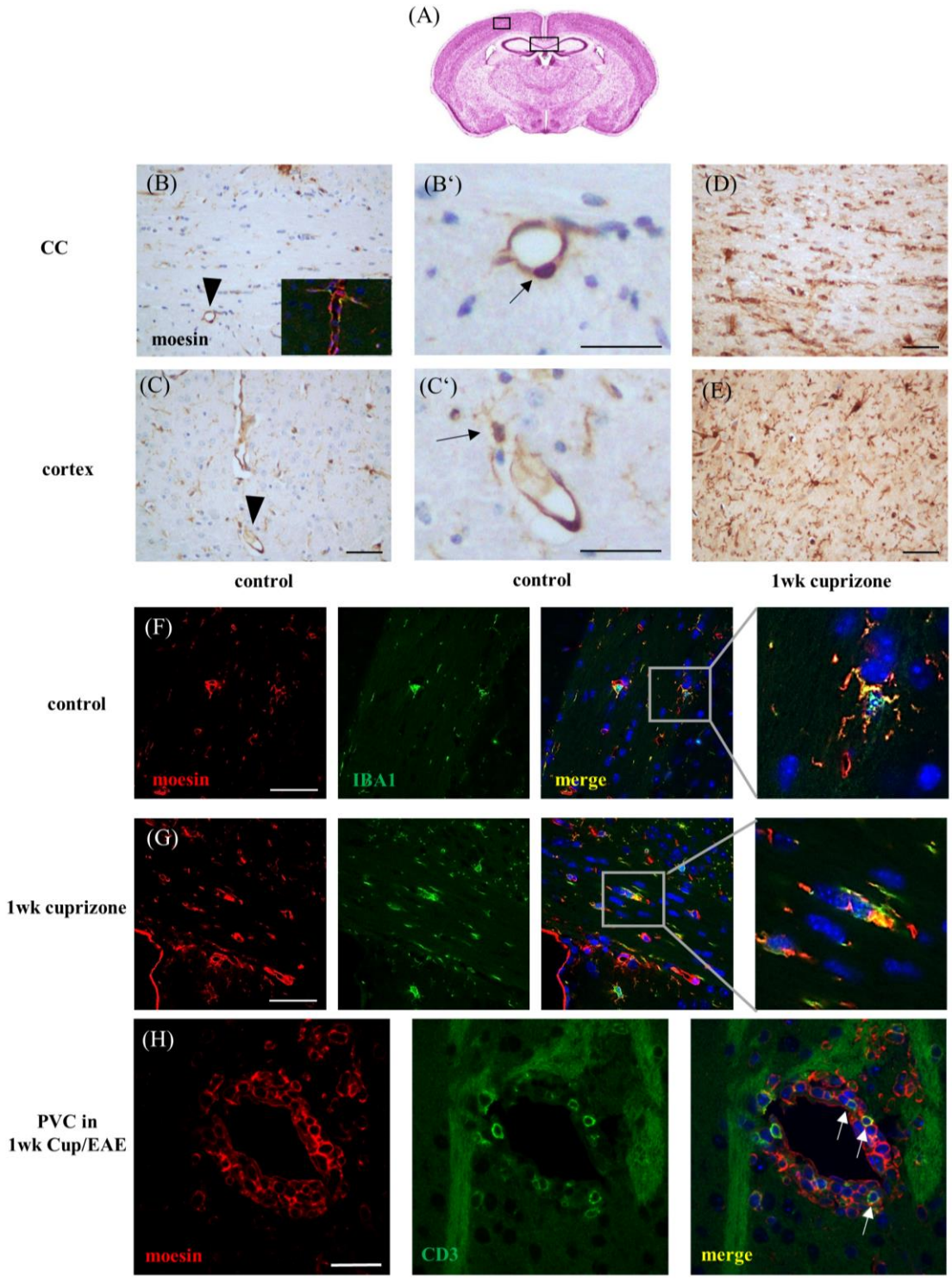

614

615 *Figure 6: Moesin expression in the cuprizone model*

616 (A) Schematic depicting the two principal regions (according to Sidman et al.) included in this part of
617 the study, namely the midline of the corpus callosum (CC) (big box) and the primary somatosensory
618 cortex area (small box). (B/B') Representative anti-moesin stain of the CC in control animals. Insert in
619 (B) shows a representative immunofluorescence double staining against CD34 (endothelial marker;
620 green) and moesin (red). The vessel shown in (B) by the arrowhead is shown in B' in higher

magnification. (C/C') Representative anti-moesin stain of the somatosensory cortex area in control animals. The vessel shown in (C) by the arrowhead is shown in C' in higher magnification. The arrow in C' highlights a moesin$^+$ microglia cell. Anti-moesin stain of the corpus callosum (D) and somatosensory cortex area (E) after 1 week cuprizone-intoxication. (F/G) Anti-ionized calcium-binding adapter molecule (IBA1) / anti-moesin immunofluorescence double stain in control (F) and 1 week cuprizone-intoxicated mice (G). Note that moesin is expressed by IBA1$^+$ microglia. (H) Anti-moesin/anti-CD3 immunofluorescence double stain in 1wk Cup/EAE mice. Note that moesin is expressed by CD3$^+$ lymphocytes (arrows).

(B-F) Scale bar: 50 µm. (B'/C'/H) Scale bar: 25 µm.

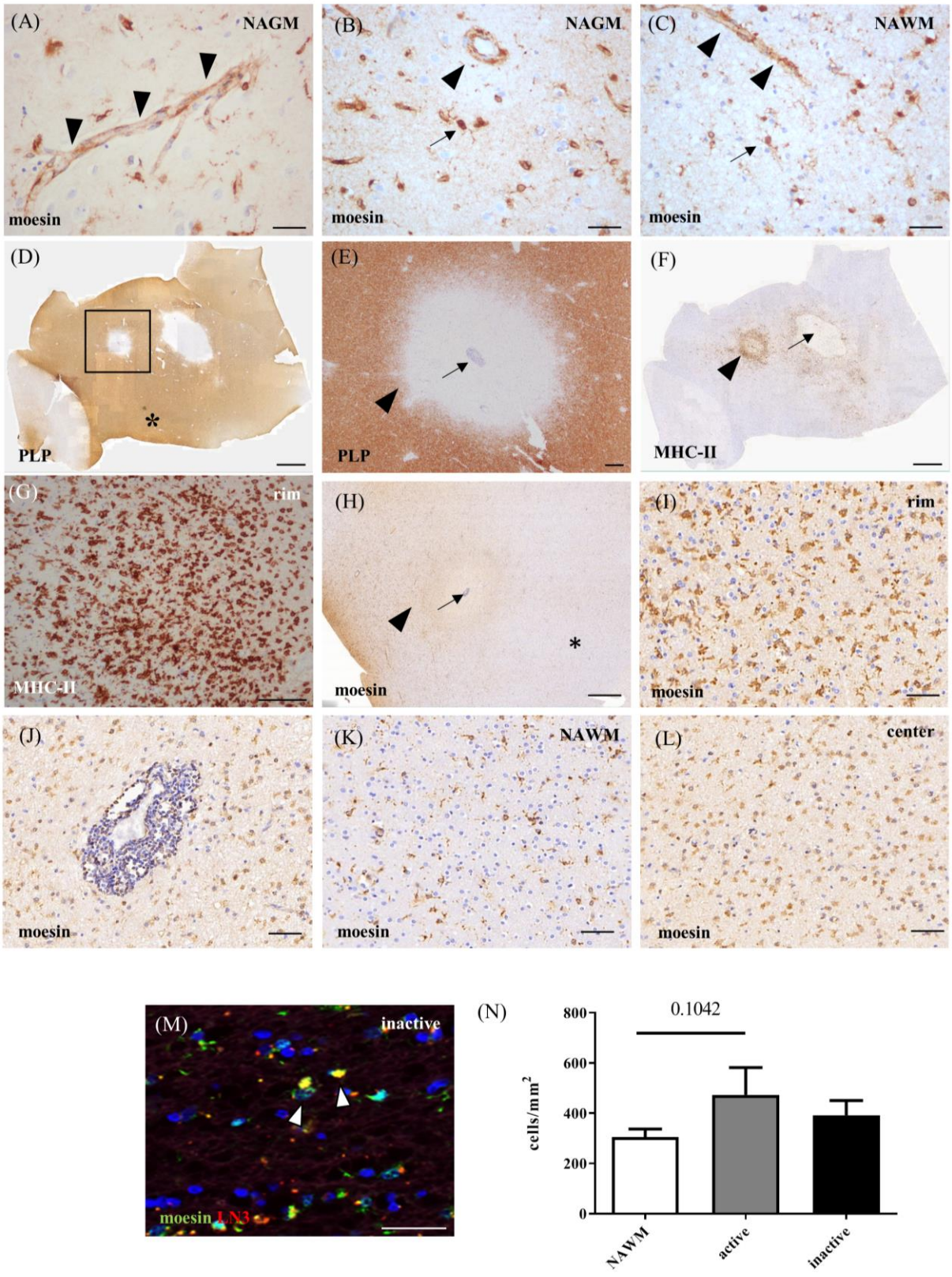

Figure 7: Moesin expression in multiple sclerosis lesions

(A/B) Representative anti-moesin stains of the normal appearing grey matter (NAGM). Arrowheads highlight a moesin$^+$ blood vessel, the arrow highlights a moesin$^+$ microglia. (C) Representative anti-

moesin stain of the normal appearing white matter (NAWM). Arrowheads highlight a moesin$^+$ blood vessel, the arrow highlights a moesin$^+$ microglia. (D) Representative anti-proteolipid protein (myelin) 1 (PLP)-stain of a chronic active lesion. Area highlighted by the box is shown in (E) in higher magnification. The star in (D) indicates NAWM. (E) The arrow highlights the center of the lesion with an inflamed vessel, the arrowhead highlights the border of the lesion. (F) Representative anti-MHC class II stain of the same section as shown in (D). The arrow highlights an inactive lesion center, the arrowhead highlights an active lesion border, which is shown in (G) in higher magnification. (H) Representative anti-moesin stain of the same section as shown in (D). The arrow highlights an inactive lesion center, the arrowhead highlights an active lesion border, the star highlights the NAWM. Moesin$^+$ cells are found at high densities at the rim of the chronic-active lesion (I) and within enlarged perivascular spaces (J). Lower densities of moesin$^+$ cells can be seen in the NAWM (K) and the inactive lesion center (L). (M) MHC-II/moesin immunofluorescence double staining of a chronic active lesion. (N) Quantification of moesin$^+$ cell densities in the normal appearing white matter (NAWM), center and border of chronic active MS lesions. Mann-Withney test was performed to compare differences between the groups.

(A-C) Scale bar: 40 µm. (D/F) Scale bar: 2 mm. (E) Scale bar: 150 µm. (G, I, J, K, L) Scale bar: 50 µm. (H) 300 µm. (M) Scale bar: 50 µm

Supplementary Tables

Supplementary Table 1: Antibodies used for immunohistochemistry and immunofluorescence

Primary antibodies							
Antigen	**Manufacturer**	**Order number**	**Host**	**Tissue**	**Dilution**	**Application**	**AGR***
ALDH1L1	Abcam	ab87117	rabbit	murine	1:2 000	Immunohistochemistry	none
APPA4	Merck-Millpore	MAB348	mouse	murine	1:5 000 1:2 500	Immunohistochemistry Immunofluorescence	Tris/EDTA
ATF3	Santa Cruz	sc-188	rabbit	murine	1:200	Immunohistochemistry	Citrat
CD3	Abcam	ab-16669	rabbit	murine	1:1 000	Immunohistochemistry	Tris/EDTA
CD3	Abcam	ab 11089	rat	murine	1:100	Immunofluorescence	Tris/EDTA
CD4	Abcam	ab-183685	rabbit	murine	1:1 000	Immunohistochemistry	Tris/EDTA
CD34	Abcam	ab8158	rat	murine	1:50	Immunofluorescence	Tris/EDTA
CNPase	Abcam	ab6313	mouse	murine	1:2 000	Immunohistochemistry	Tris/EDTA
GFAP	Abcam	ab4674	chicken	murine	1:8 000	Immunohistochemistry	Tris/EDTA
IBA1	Abcam	Ab107159	goat	murine	1:1 000	Immunofluorescence	Tris/EDTA
IBA1	Wako	019-19 741	rabbit	murine	1:5 000	Immunohistochemistry	Tris/EDTA
MAG	Abcam	ab89780	mouse	murine	1:4 000	Immunohistochemistry	Citrat
MHC-II	Thermo-Fisher Scientific	MA5-11966	mouse	human	1:1 500 1:800	Immunohistochemistry Immunofluorescence	Citrat
Moesin	Abcam	ab151542	rabbit	murine murine human	1:250 1:100 1:250 1:100	Immunohistochemistry Immunofluorescence Immunohistochemistry Immunofluorescence	Tris/EDTA Citrat Tris/EDTA Citrat
PLP	Abcam	MCA-839G	mouse	murine human	1:5 000	Immunohistochemistry	none
Biotinylated secondary antibodies							
goat anti-mouse IgG	Vector	BA-9200	goat		1:200		not applicable
goat anti-rabbit IgG	Vector	BA-1000	goat		1:200		not applicable
goat anti-chicken IgG	Vector	BA-9010	goat		1:200		not applicable
Flourescent secondary antibodies							
Alexa 488	Invitrogen/Life Technologie	A21202	donkey anti-mouse		1:1 000		not applicable
Alexa 488	Invitrogen/Life Technologie	A11055	donkey anti-goat		1:200		not applicable
Alexa 594	Invitrogen/Life Technologie	A21207	donkey anti-rabbit		1:200		not applicable
Alexa 594	Invitrogen/Life Technologie	A21203	donkey anti-mouse		1:200		not applicable
Alexa 488	Invitrogen/Life Technologie	A21206	donkey anti-rabbit		1:200		not applicable
Alexa 488	Invitrogen/Life Technologie	A21208	donkey anti-rat		1:200		not applicable
Isotype			Conentration Isotype	Primary antibody	Dilution		
IgG2a	Abcam	ab18415	0.5mg/ml	PLP	1:2 500	Immunohistochemistry	
IgG1	Abcam	ab18443	0.5mg/ml	APPA4	1:2 500	Immunohistochemistry	
*antigen retrieval							

653 Supplementary Table 2: List of genes with induced und reduced expression in the corpus callosum of
654 cuprizone-intoxicated mice

Gene Symbol	Affy ProbeSet ID	con Avg (log2)	con S.D.	cuprizone Avg (log2)	cuprizone S.D.	Fold Change cuprizone vs control (log2)	FDR P-val con vs cuprizone
Mog	10450845	11,12	0,12	7,34	0,45	3,78136	2,05E-06
Mag	10562152	11,52	0,12	8,33	0,49	3,19061	6,47E-06
Mal	10487441	11,48	0,17	8,35	0,4	3,13586	3,77E-06
Aspa	10388254	9,18	0,25	6,37	0,48	2,81352	2,55E-05
Fa2h	10581824	10,39	0,09	7,81	0,29	2,57773	2,05E-06
Tmem88b	10519203	9,95	0,19	7,55	0,29	2,40599	3,77E-06
Ugt8a	10501963	11,16	0,13	8,91	0,28	2,24793	3,89E-06
Ppp1r14a	10551736	9,36	0,22	7,18	0,18	2,17632	2,83E-06
Tspan2	10494821	11,25	0,19	9,11	0,48	2,14405	9,65E-05
Cldn11	10491313	11,67	0,11	9,63	0,29	2,03914	4,72E-06
Opalin	10467529	9,39	0,15	7,43	0,58	1,95606	0,0004
Klk6	10552516	8,78	0,06	6,91	0,07	1,87184	1,95E-07
Gamt	10370766	9,56	0,15	7,73	0,07	1,82375	1,71E-06
S1pr5	10591494	9,02	0,32	7,23	0,17	1,79077	2,91E-05
Efhd1	10348194	9,92	0,16	8,14	0,16	1,77821	2,27E-06
Anln	10591781	9,07	0,07	7,3	0,37	1,76977	4,40E-05
Trf	10596148	11,53	0,22	9,79	0,48	1,73985	0,0003
Ermn	10482795	10,59	0,14	8,88	0,49	1,70929	0,0001
Cyp2j12	10514491	8,16	0,19	6,5	0,26	1,65992	3,09E-05
Plekhh1	10396800	8,78	0,12	7,13	0,41	1,65076	0,0002
Padi2	10509838	8,91	0,09	7,26	0,18	1,64616	3,19E-06
Adamts4	10351551	8,97	0,16	7,35	0,17	1,61353	8,22E-06
Hapln2	10499299	8,58	0,05	6,98	0,21	1,60407	5,64E-06
Cnp	10381154	11,85	0,14	10,26	0,28	1,58976	3,49E-05
Cmtm5	10415132	11,33	0,15	9,75	0,38	1,57531	0,0002
Ninj2	10541206	8,13	0,16	6,56	0,26	1,57046	4,63E-05
Galnt6	10432661	7,34	0,18	5,78	0,21	1,56071	3,16E-05
Plp1	10601888	13,41	0,11	11,86	0,3	1,54597	4,45E-05
Pllp	10580765	9,53	0,16	8,02	0,22	1,50080	2,45E-05
Car14	10500283	8,28	0,06	6,79	0,15	1,49057	2,10E-06
Erbb3	10373467	8,51	0,14	7,03	0,15	1,48027	8,22E-06
Sept4	10380067	10,42	0,15	8,95	0,17	1,46989	1,50E-05
Ttyh2	10382376	10,46	0,07	9,01	0,21	1,44890	9,76E-06
Mobp	10590269	11,65	0,12	10,22	0,47	1,43296	0,0005
Qdpr	10529895	11,25	0,13	9,81	0,27	1,43296	7,32E-05
Prr5l	10485378	7,55	0,09	6,12	0,32	1,42761	0,0001
Tmem63a	10352320	9,55	0,15	8,15	0,25	1,40054	4,21E-05
Nipal4	10385384	8,1	0,1	6,71	0,12	1,39506	2,27E-06
Plekhb1	10565910	11,95	0,05	10,58	0,25	1,37295	4,40E-05
Lpar1	10513256	9,66	0,12	8,29	0,12	1,36737	4,43E-06
Unc5b	10369388	8,7	0,1	7,36	0,19	1,34483	1,53E-05
Carns1	10464642	8,5	0,08	7,16	0,14	1,33914	6,89E-06
Plxnb3	10600249	9,02	0,1	7,69	0,05	1,32769	2,05E-06
Il33	10462442	9,41	0,21	8,09	0,34	1,31615	0,0005
Gjb1	10601161	7,61	0,24	6,35	0,32	1,26903	0,0004
Cntn2	10357705	9,96	0,07	8,7	0,1	1,26303	2,10E-06
Phldb1	10592891	9,6	0,17	8,35	0,1	1,24489	1,50E-05
Mbp	10457022	12,22	0,08	10,99	0,22	1,23266	3,56E-05
Cpm	10366546	8,32	0,13	7,11	0,25	1,20789	0,0001
Prr18	10441657	8,52	0,15	7,31	0,07	1,20789	8,22E-06
Efnb3	10387483	9,59	0,17	8,41	0,13	1,17632	2,99E-05
Smco3	10548871	8,3	0,07	7,12	0,32	1,17632	0,0001
Gsn	10471655	8,91	0,19	7,75	0,1	1,15704	4,07E-05
Mob3b	10512022	8,58	0,1	7,43	0,21	1,15056	5,80E-05
Pigz	10434993	9,21	0,12	8,06	0,18	1,14405	4,25E-05
Ccp110	10556640	9,58	0,06	8,44	0,04	1,13750	2,05E-06
Pde8a	10554521	8,94	0,18	7,8	0,1	1,13750	2,99E-05
Gm22290	10416897	4,27	0,54	3,15	0,37	1,11770	0,0302
Lrrn1	10540401	10,68	0,08	9,59	0,07	1,09761	3,77E-06
Apln	10604375	9,08	0,05	8	0,28	1,08406	0,0005
Myrf	10465916	9,6	0,1	8,52	0,28	1,07724	0,0004
D7Ertd443e	10568696	7,8	0,11	6,74	0,21	1,05658	0,0001
Fam57a	10378754	9,78	0,08	8,72	0,1	1,05658	1,26E-05
Ptgds	10480734	11,25	0,12	10,19	0,46	1,05658	0,0062
Cers2	10494227	10,22	0,15	9,17	0,2	1,04963	0,0002
Cd82	10485213	9,65	0,24	8,62	0,26	1,03562	0,0009
Cryab	10585214	11,59	0,09	10,56	0,16	1,03562	4,40E-05
Elovl7	10407072	9,14	0,18	8,11	0,19	1,03562	0,0002
Prrg1	10605493	7,53	0,1	6,5	0,08	1,02857	8,22E-06
Enpp2	10428619	11,75	0,28	10,74	0,57	1,00000	0,0252
Rhog	10566132	9,61	0,1	8,61	0,16	1,00000	9,84E-05
Gjc3	10534960	11,15	0,07	10,16	0,3	0,99277	0,0007
Sgk2	10478326	7,22	0,13	6,23	0,29	0,99277	0,0005
Gstm7	10501199	9,23	0,16	8,24	0,19	0,98550	0,0002
Mboat1	10404359	7,42	0,18	6,43	0,11	0,98550	6,44E-05
Mcam	10584674	9,25	0,07	8,27	0,13	0,97820	2,62E-05
vi2a; Evi2b; Gm2197	10388958	8,41	0,14	7,43	0,21	0,97085	0,0004

vi2a; Evi2b; Gm2197	10388958	8,41	0,14	7,43	0,21	0,97085	0,0004
Map6d1	10438456	10,26	0,06	9,3	0,03	0,97085	4,00E-06
Slc12a2	10455873	10,15	0,17	9,18	0,23	0,97085	0,0006
Plekhg3	10396671	8,1	0,19	7,13	0,18	0,96347	0,0006
Scd1	10467979	11,33	0,07	10,37	0,19	0,96347	9,84E-05
Tprn	10469957	7,82	0,06	6,85	0,12	0,96347	2,03E-05
Dock5	10421046	8,49	0,14	7,53	0,16	0,95606	0,0001
Trim59	10498620	7,88	0,25	6,92	0,33	0,95606	0,0043
Lgi3	10416279	10,97	0,12	10,02	0,23	0,94111	0,0002
Sh3gl3	10554588	9,3	0,15	8,37	0,13	0,93357	0,0002
Tppp3	10581266	9,87	0,15	8,93	0,18	0,93357	0,0003
Josd2	10552681	9,62	0,11	8,7	0,11	0,91839	6,40E-05
Tmem98	10379489	7,93	0,16	7,02	0,18	0,91839	0,0001
Hhip	10579894	8,33	0,18	7,42	0,16	0,91073	0,0003
Desi1	10430804	11,28	0,08	10,37	0,1	0,90304	2,81E-05
Trim13	10415784	9,32	0,1	8,42	0,08	0,90304	3,53E-05
Gjc2	10386352	7,93	0,09	7,04	0,09	0,89530	2,45E-05
Gm10863	10425265	7,84	0,18	6,95	0,04	0,89530	0,0001
Gm38481; Idi1	10482762	9,79	0,12	8,9	0,11	0,89530	6,42E-05
Idi1	10403413	10,02	0,15	9,13	0,11	0,88753	0,0001
Pacs2	10398936	10,29	0,08	9,4	0,17	0,88753	0,0002
Prkcq	10469255	8,68	0,14	7,79	0,12	0,88753	6,42E-05
Elovl1	10507539	9,67	0,15	8,8	0,18	0,87184	0,0011
Olfml1	10556076	7,91	0,15	7,05	0,23	0,86394	0,0004
Slc7a10	10552143	9,46	0,07	8,59	0,28	0,86394	0,0019
St18	10344679	8,06	0,23	7,19	0,32	0,86394	0,0022
Abca2	10470050	10,63	0,06	9,79	0,12	0,84800	4,08E-05
Ebp	10603485	8,73	0,06	7,88	0,13	0,84800	4,45E-05
Gatm	10487011	11,89	0,13	11,04	0,25	0,84800	0,0009
Bche	10498710	6,83	0,07	5,99	0,19	0,83996	0,0002
Cdc42ep2	10465278	8,85	0,11	8	0,09	0,83996	5,55E-05
Sytl2	10554863	9,51	0,08	8,67	0,04	0,83996	1,50E-05
Abca8a	10392522	5,94	0,11	5,11	0,18	0,83188	0,0003
Pla2g16	10461093	8,24	0,17	7,42	0,24	0,83188	0,0021
Sec14l5	10433373	7,61	0,13	6,78	0,24	0,83188	0,0009
Srd5a1	10410452	8,3	0,09	7,48	0,06	0,82375	2,99E-05
Dbndd2	10478495	8,73	0,08	7,92	0,13	0,81558	8,91E-05
Gm9791	10497752	9,38	0,14	8,57	0,1	0,81558	0,0003
Ctnna3	10363676	6,81	0,09	6	0,2	0,80735	0,0005
Mfge8	10564713	9,61	0,07	8,8	0,13	0,80735	6,44E-05
Mir219a-2; Gm3088	10481378	7,38	0,14	6,57	0,13	0,80735	0,0007
Rtkn2	10363743	6,65	0,1	5,85	0,09	0,80735	6,42E-05
Shtn1	10468762	9,23	0,09	8,42	0,15	0,80735	0,0001
Nmral1	10437432	7,71	0,18	6,91	0,06	0,79909	0,0003
Ano4	10371740	8,79	0,09	7,99	0,1	0,79077	6,42E-05
Rffl	10389087	8,42	0,02	7,63	0,12	0,79077	4,40E-05
Ldlr	10583732	8,76	0,13	7,98	0,08	0,78241	0,0002
Pls1	10595768	8,24	0,07	7,46	0,22	0,78241	0,0007
Arhgap23	10380773	9,37	0,11	8,59	0,03	0,77400	5,15E-05
Car2	10490923	11,35	0,14	10,58	0,28	0,77400	0,0074
Gng8	10550388	6,81	0,11	6,03	0,1	0,77400	0,0002
Mir100	10584589	6,24	0,19	5,47	0,3	0,77400	0,0077
Ankub1	10498302	7,44	0,13	6,67	0,36	0,76553	0,0041
Apod	10439009	12,02	0,07	11,26	0,16	0,76553	0,0004
Clmn	10402473	9,33	0,13	8,57	0,37	0,76553	0,0383
Insig1	10520362	9,88	0,24	9,12	0,18	0,76553	0,0017
Map7	10361956	9,63	0,07	8,87	0,08	0,76553	4,21E-05
Gstm5	10495243	10,05	0,19	9,3	0,1	0,75702	0,0009
Adssl1	10398859	8,54	0,21	7,79	0,2	0,74846	0,0014
Bcas1	10490061	10,21	0,15	9,46	0,21	0,74846	0,0016
Gm9895	10462343	6,94	0,22	6,19	0,16	0,74846	0,0019
Hmgcs1	10412466	10,5	0,11	9,75	0,06	0,74846	8,44E-05
Kctd4	10416505	7,52	0,17	6,77	0,18	0,74846	0,0007
Lrp4	10473880	8,81	0,13	8,07	0,05	0,74846	0,0001
Myo1d	10389022	8,87	0,15	8,12	0,2	0,74846	0,0013
Slc44a1	10505008	10,67	0,11	9,92	0,04	0,74846	9,84E-05
Enpp6	10571715	8,46	0,08	7,72	0,1	0,73985	9,84E-05
Sp7	10433003	6,55	0,24	5,81	0,2	0,73985	0,0025
Usp54	10417920	9,37	0,11	8,63	0,16	0,73985	0,0006
Chil1	10349968	7,81	0,15	7,07	0,37	0,73118	0,0147
Gpr37	10543466	9,87	0,18	9,15	0,38	0,73118	0,0066
Nkain2	10368585	10,98	0,04	10,26	0,14	0,72247	0,0003
Pmp22	10376950	10,43	0,02	9,71	0,23	0,72247	0,0018
St6galnac3	10502890	8,25	0,1	7,52	0,03	0,72247	6,40E-05
Tnni1	10350149	7,65	0,14	6,93	0,19	0,72247	0,0007
Fah	10565315	8,82	0,12	8,11	0,19	0,71370	0,0011
Ndrg1	10429140	10,89	0,04	10,18	0,25	0,71370	0,0041
Rnf122	10571214	8,92	0,08	8,21	0,1	0,71370	0,0001

Sccpdh	10352178	9,5	0,2	8,78	0,23	0,71370	0,0088
Enpp1	10368289	7,76	0,07	7,06	0,11	0,70487	0,0002
Itgb4	10382713	7,82	0,12	7,12	0,19	0,70487	0,0010
Tppp	10406171	10,83	0,05	10,13	0,05	0,70487	3,16E-05
Adamtsl4	10500183	8,08	0,1	7,38	0,1	0,69599	0,0001
Pik3c2b	10349834	9,56	0,01	8,87	0,1	0,69599	6,63E-05
Tmeff1	10504891	10,5	0,08	9,81	0,12	0,69599	0,0004
Carhsp1	10437590	8,68	0,15	7,99	0,14	0,68706	0,0006
Dhcr7	10559312	9,02	0,1	8,34	0,14	0,68706	0,0005
Myo1d	10389025	9,2	0,21	8,51	0,15	0,68706	0,0008
Pip4k2a	10480347	10,85	0,12	10,16	0,12	0,68706	0,0007
Dhcr24	10506571	9,92	0,12	9,24	0,17	0,67807	0,0015
Hopx	10530819	8,47	0,22	7,79	0,03	0,67807	0,0013
Sema4d	10409236	9,67	0,06	9	0,11	0,67807	0,0002
Usp54	10417912	10,23	0,08	9,55	0,18	0,67807	0,0010
Foxn3	10402063	9,69	0,14	9,02	0,13	0,66903	0,0017
Gal3st1	10373826	7,4	0,07	6,73	0,13	0,66903	0,0005
Kndc1	10558548	9,97	0,12	9,3	0,24	0,66903	0,0047
Rasgrp3	10446965	8,74	0,09	8,07	0,11	0,66903	0,0002
Myoc	10351131	6,37	0,18	5,72	0,33	0,65992	0,0209
Nrbp2	10429754	10,92	0,08	10,26	0,18	0,65992	0,0018
Rcbtb1	10415662	9,59	0,08	8,93	0,04	0,65992	7,32E-05
Smad7	10456745	8,69	0,16	8,04	0,11	0,65992	0,0031
Thbs4	10411082	8,79	0,21	8,13	0,33	0,65992	0,0267
Tubb4a	10452295	12,25	0,01	11,59	0,09	0,65992	6,43E-05
B3galt5	10437191	8,7	0,13	8,04	0,12	0,65076	0,0006
Daam2	10451679	8,93	0,19	8,28	0,23	0,65076	0,0056
Polr3e	10557058	8,54	0,13	7,89	0,22	0,65076	0,0033
Cacna2d4	10541144	7,22	0,2	6,58	0,23	0,64155	0,0162
Cdk18	10357676	9,25	0,13	8,61	0,18	0,64155	0,0017
Cyp27a1	10347481	8,17	0,09	7,52	0,13	0,64155	0,0004
Cyp51	10527920	9,1	0,1	8,46	0,07	0,64155	0,0002
Klhl4	10601519	8,72	0,16	8,08	0,4	0,64155	0,0188
Plpp2	10370552	8,56	0,14	7,92	0,12	0,64155	0,0005
Slc4a2	10520187	8,64	0,15	8	0,04	0,64155	0,0010
Csrp1	10350136	11,96	0,07	11,33	0,14	0,63227	0,0005
Fam83d	10478160	6,74	0,18	6,1	0,04	0,63227	0,0011
Prima1	10402318	8,19	0,08	7,55	0,16	0,63227	0,0011
Ptprd	10513957	11,35	0,05	10,72	0,14	0,63227	0,0008
Sema4d	10409240	9,28	0,07	8,64	0,12	0,63227	0,0005
Sorbs3	10421269	8,52	0,08	7,89	0,09	0,63227	0,0003
Trp53inp2	10477644	11,08	0,05	10,44	0,11	0,63227	0,0002
Plekhf1	10562576	7,49	0,3	6,86	0,2	0,62293	0,0161
Tmem125	10515797	7,42	0,11	6,8	0,17	0,62293	0,0029
Gpr62	10596489	7,93	0,13	7,32	0,14	0,61353	0,0019
Il17rb	10418341	6,82	0,06	6,21	0,12	0,61353	0,0007
Nfe2l3	10538275	7,56	0,1	6,95	0,1	0,61353	0,0002
Ranbp3l	10422946	5,99	0,06	5,37	0,16	0,61353	0,0011
Rhou	10576386	9,71	0,14	9,09	0,14	0,61353	0,0041
Zdhhc9	10604380	10,23	0,07	9,62	0,12	0,61353	0,0004
March8	10541049	9,11	0,07	8,5	0,18	0,60407	0,0013
Sox8	10448967	9,9	0,04	9,3	0,06	0,60407	9,38E-05
Tmem229a	10543460	8,71	0,17	8,11	0,17	0,60407	0,0259
Trim13	10395198	7,32	0,09	6,71	0,08	0,60407	0,0003
Gpc5	10416960	8,15	0,1	7,55	0,15	0,59455	0,0014
Jam3	10591967	8,24	0,15	7,65	0,17	0,59455	0,0041
Marcksl1	10508465	8,14	0,15	7,55	0,15	0,59455	0,0012
Nkx2-9	10400479	7,21	0,06	6,61	0,2	0,59455	0,0027
Plxnb1	10589368	9,18	0,06	8,58	0,15	0,59455	0,0020
Rlbp1	10564726	7,51	0,09	6,92	0,05	0,59455	0,0002
Slc1a2	10474141	12,12	0,09	11,53	0,1	0,59455	0,0005
Tspan15	10369531	8,2	0,19	7,61	0,11	0,59455	0,0035
Atp8b1	10459421	7,44	0,09	6,85	0,14	0,58496	0,0012
Bpgm	10537179	7,86	0,15	7,27	0,24	0,58496	0,0086

References

Acs, P., M. Kipp, A. Norkute, S. Johann, T. Clarner, A. Braun, Z. Berente, S. Komoly and C. Beyer (2009). "17beta-estradiol and progesterone prevent cuprizone provoked demyelination of corpus callosum in male mice." Glia **57**(8): 807-814.

Acs, P. and S. Komoly (2012). "Selective ultrastructural vulnerability in the cuprizone-induced experimental demyelination." Ideggyogy Sz **65**(7-8): 266-270.

Ansa-Addo, E. A., Y. Zhang, Y. Yang, G. S. Hussey, B. V. Howley, M. Salem, B. Riesenberg, S. Sun, D. C. Rockey, S. Karvar, P. H. Howe, B. Liu and Z. Li (2017). "Membrane-organizing protein moesin controls Treg differentiation and antitumor immunity via TGF-beta signaling." J Clin Invest **127**(4): 1321-1337.

Barnett, M. H. and J. W. Prineas (2004). "Relapsing and remitting multiple sclerosis: pathology of the newly forming lesion." Ann Neurol **55**(4): 458-468.

Bauer, J., H. Rauschka and H. Lassmann (2001). "Inflammation in the nervous system: the human perspective." Glia **36**(2): 235-243.

Benn, T., C. Halfpenny and N. Scolding (2001). "Glial cells as targets for cytotoxic immune mediators." Glia **36**(2): 200-211.

Berryman, M., Z. Franck and A. Bretscher (1993). "Ezrin is concentrated in the apical microvilli of a wide variety of epithelial cells whereas moesin is found primarily in endothelial cells." J Cell Sci **105 (Pt 4)**: 1025-1043.

Bogdanove, L. H. and G. Clark (1957). "The induction of exacerbations of allergic meningoencephalomyelitis." J Neuropathol Exp Neurol **16**(1): 57-60.

Buschmann, J. P., K. Berger, H. Awad, T. Clarner, C. Beyer and M. Kipp (2012). "Inflammatory response and chemokine expression in the white matter corpus callosum and gray matter cortex region during cuprizone-induced demyelination." J Mol Neurosci **48**(1): 66-76.

Clark, G. and L. H. Bogdanove (1955). "The induction of the lesions of allergic meningoencephalomyelitis in a predetermined location." J Neuropathol Exp Neurol **14**(4): 433-437.

Clarner, T., F. Diederichs, K. Berger, B. Denecke, L. Gan, P. van der Valk, C. Beyer, S. Amor and M. Kipp (2012). "Myelin debris regulates inflammatory responses in an experimental demyelination animal model and multiple sclerosis lesions." Glia **60**(10): 1468-1480.

Clarner, T., K. Janssen, L. Nellessen, M. Stangel, T. Skripuletz, B. Krauspe, F. M. Hess, B. Denecke, C. Beutner, B. Linnartz-Gerlach, H. Neumann, L. Vallieres, S. Amor, K. Ohl, K. Tenbrock, C. Beyer and M. Kipp (2015). "CXCL10 triggers early microglial activation in the cuprizone model." J Immunol **194**(7): 3400-3413.

De Groot, C. J., E. Bergers, W. Kamphorst, R. Ravid, C. H. Polman, F. Barkhof and P. van der Valk (2001). "Post-mortem MRI-guided sampling of multiple sclerosis brain lesions: increased yield of active demyelinating and (p)reactive lesions." Brain **124**(Pt 8): 1635-1645.

Fehon, R. G., A. I. McClatchey and A. Bretscher (2010). "Organizing the cell cortex: the role of ERM proteins." Nat Rev Mol Cell Biol **11**(4): 276-287.

Ferguson, B., M. K. Matyszak, M. M. Esiri and V. H. Perry (1997). "Axonal damage in acute multiple sclerosis lesions." Brain **120 (Pt 3)**: 393-399.

Filippi, M., M. A. Rocca, G. Martino, M. A. Horsfield and G. Comi (1998). "Magnetization transfer changes in the normal appearing white matter precede the appearance of enhancing lesions in patients with multiple sclerosis." Ann Neurol **43**(6): 809-814.

Fischbach, F., J. Nedelcu, P. Leopold, J. Zhan, T. Clarner, L. Nellessen, C. Beissel, Y. van Heuvel, A. Goswami, J. Weis, B. Denecke, C. Schmitz, T. Hochstrasser, S. Nyamoya, M. Victor, C. Beyer and M. Kipp (2018). "Cuprizone-induced graded oligodendrocyte vulnerability is regulated by the transcription factor DNA damage-inducible transcript 3." Glia.

Goldberg, J., M. Daniel, Y. van Heuvel, M. Victor, C. Beyer, T. Clarner and M. Kipp (2013). "Short-term cuprizone feeding induces selective amino acid deprivation with concomitant activation of an integrated stress response in oligodendrocytes." Cell Mol Neurobiol **33**(8): 1087-1098.

706 Grosse-Veldmann, R., B. Becker, S. Amor, P. van der Valk, C. Beyer and M. Kipp (2016). "Lesion
707 Expansion in Experimental Demyelination Animal Models and Multiple Sclerosis Lesions." Mol
708 Neurobiol **53**(7): 4905-4917.
709 Hagemeier, K., A. Lurbke, S. Hucke, S. Albrecht, A. Preisner, E. Klassen, E. Hoffmann, Q. L. Cui, J. J. Antel,
710 W. Bruck, L. Klotz and T. Kuhlmann (2013). "Puma, but not noxa is essential for oligodendroglial cell
711 death." Glia **61**(10): 1712-1723.
712 Haider, L., M. T. Fischer, J. M. Frischer, J. Bauer, R. Hoftberger, G. Botond, H. Esterbauer, C. J. Binder,
713 J. L. Witztum and H. Lassmann (2011). "Oxidative damage in multiple sclerosis lesions." Brain **134**(Pt
714 7): 1914-1924.
715 Hardy, T. A., W. O. Tobin and C. F. Lucchinetti (2016). "Exploring the overlap between multiple sclerosis,
716 tumefactive demyelination and Balo's concentric sclerosis." Mult Scler **22**(8): 986-992.
717 Henderson, A. P., M. H. Barnett, J. D. Parratt and J. W. Prineas (2009). "Multiple sclerosis: distribution
718 of inflammatory cells in newly forming lesions." Ann Neurol **66**(6): 739-753.
719 Hoflich, K. M., C. Beyer, T. Clarner, C. Schmitz, S. Nyamoya, M. Kipp and T. Hochstrasser (2016). "Acute
720 axonal damage in three different murine models of multiple sclerosis: A comparative approach." Brain
721 Res **1650**: 125-133.
722 Iglesias, A., J. Bauer, T. Litzenburger, A. Schubart and C. Linington (2001). "T- and B-cell responses to
723 myelin oligodendrocyte glycoprotein in experimental autoimmune encephalomyelitis and multiple
724 sclerosis." Glia **36**(2): 220-234.
725 Irizarry, R. A., B. Hobbs, F. Collin, Y. D. Beazer-Barclay, K. J. Antonellis, U. Scherf and T. P. Speed (2003).
726 "Exploration, normalization, and summaries of high density oligonucleotide array probe level data."
727 Biostatistics **4**(2): 249-264.
728 Janssen, K., M. Rickert, T. Clarner, C. Beyer and M. Kipp (2016). "Absence of CCL2 and CCL3 Ameliorates
729 Central Nervous System Grey Matter But Not White Matter Demyelination in the Presence of an Intact
730 Blood-Brain Barrier." Mol Neurobiol **53**(3): 1551-1564.
731 Kashimoto, R., H. Yamanaka, K. Kobayashi, M. Okubo, H. Yagi, O. Mimura and K. Noguchi (2013).
732 "Phosphorylation of ezrin/radixin/moesin (ERM) protein in spinal microglia following peripheral nerve
733 injury and lysophosphatidic acid administration." Glia **61**(3): 338-348.
734 Konno, H., T. Yamamoto, H. Suzuki, H. Yamamoto, Y. Iwasaki, Y. Ohara, H. Terunuma and N. Harata
735 (1990). "Targeting of adoptively transferred experimental allergic encephalitis lesion at the sites of
736 wallerian degeneration." Acta Neuropathol **80**(5): 521-526.
737 Kornek, B., M. K. Storch, R. Weissert, E. Wallstroem, A. Stefferl, T. Olsson, C. Linington, M. Schmidbauer
738 and H. Lassmann (2000). "Multiple sclerosis and chronic autoimmune encephalomyelitis: a
739 comparative quantitative study of axonal injury in active, inactive, and remyelinated lesions." Am J
740 Pathol **157**(1): 267-276.
741 Krauspe, B. M., W. Dreher, C. Beyer, W. Baumgartner, B. Denecke, K. Janssen, C. D. Langhans, T. Clarner
742 and M. Kipp (2015). "Short-term cuprizone feeding verifies N-acetylaspartate quantification as a
743 marker of neurodegeneration." J Mol Neurosci **55**(3): 733-748.
744 Lake, J., R. O. Weller, M. J. Phillips and M. Needham (1999). "Lymphocyte targeting of the brain in
745 adoptive transfer cryolesion-EAE." J Pathol **187**(2): 259-265.
746 Levine, S. (1960). "Localization of allergic encephalomyelitis in lesions of cyanide encephalopathy." J
747 Neuropathol Exp Neurol **19**: 238-247.
748 Levine, S. and E. M. Hoenig (1968). "Induced localization of allergic adrenalitis and encephalomyelitis
749 at sites of thermal injury." J Immunol **100**(6): 1310-1318.
750 Levine, S. and E. M. Hoenig (1971). "A new form of localized allergic encephalomyelitis featuring
751 polymorphonuclear neutrophilic leukocytes." Am J Pathol **64**(1): 13-30.
752 Levine, S. and E. J. Wenk (1967). "Rapid passive transfer of allergic encephalomyelitis." J Immunol
753 **99**(6): 1277-1285.
754 Levine, S., H. M. Zimmerman, E. J. Wenk and N. K. Gonatas (1963). "Experimental
755 leukoencephalopathies due to implantation of foreign substances." Am J Pathol **42**: 97-117.
756 Lublin, F. D., S. C. Reingold, J. A. Cohen, G. R. Cutter, P. S. Sorensen, A. J. Thompson, J. S. Wolinsky, L. J.
757 Balcer, B. Banwell, F. Barkhof, B. Bebo, Jr., P. A. Calabresi, M. Clanet, G. Comi, R. J. Fox, M. S. Freedman,

A. D. Goodman, M. Inglese, L. Kappos, B. C. Kieseier, J. A. Lincoln, C. Lubetzki, A. E. Miller, X. Montalban, P. W. O'Connor, J. Petkau, C. Pozzilli, R. A. Rudick, M. P. Sormani, O. Stuve, E. Waubant and C. H. Polman (2014). "Defining the clinical course of multiple sclerosis: the 2013 revisions." Neurology **83**(3): 278-286.

Lucchinetti, C., W. Bruck, J. Parisi, B. Scheithauer, M. Rodriguez and H. Lassmann (2000). "Heterogeneity of multiple sclerosis lesions: implications for the pathogenesis of demyelination." Ann Neurol **47**(6): 707-717.

Maggi, P., S. M. Macri, M. I. Gaitan, E. Leibovitch, J. E. Wholer, H. L. Knight, M. Ellis, T. Wu, A. C. Silva, L. Massacesi, S. Jacobson, S. Westmoreland and D. S. Reich (2014). "The formation of inflammatory demyelinated lesions in cerebral white matter." Ann Neurol **76**(4): 594-608.

Mana, P., S. A. Fordham, M. A. Staykova, M. Correcha, D. Silva, D. O. Willenborg and D. Linares (2009). "Demyelination caused by the copper chelator cuprizone halts T cell mediated autoimmune neuroinflammation." J Neuroimmunol **210**(1-2): 13-21.

Marik, C., P. A. Felts, J. Bauer, H. Lassmann and K. J. Smith (2007). "Lesion genesis in a subset of patients with multiple sclerosis: a role for innate immunity?" Brain **130**(Pt 11): 2800-2815.

Moon, Y., J. Y. Kim, S. Y. Choi, K. Kim, H. Kim and W. Sun (2011). "Induction of ezrin-radixin-moesin molecules after cryogenic traumatic brain injury of the mouse cortex." Neuroreport **22**(6): 304-308.

Narayana, P. A., T. J. Doyle, D. Lai and J. S. Wolinsky (1998). "Serial proton magnetic resonance spectroscopic imaging, contrast-enhanced magnetic resonance imaging, and quantitative lesion volumetry in multiple sclerosis." Ann Neurol **43**(1): 56-71.

Nimmerjahn, A., F. Kirchhoff and F. Helmchen (2005). "Resting microglial cells are highly dynamic surveillants of brain parenchyma in vivo." Science **308**(5726): 1314-1318.

Noell, S., K. Wolburg-Buchholz, A. F. Mack, R. Ritz, M. Tatagiba, R. Beschorner, H. Wolburg and P. Fallier-Becker (2012). "Dynamics of expression patterns of AQP4, dystroglycan, agrin and matrix metalloproteinases in human glioblastoma." Cell Tissue Res **347**(2): 429-441.

Nomachi, A., M. Yoshinaga, J. Liu, P. Kanchanawong, K. Tohyama, D. Thumkeo, T. Watanabe, S. Narumiya and T. Hirata (2013). "Moesin controls clathrin-mediated S1PR1 internalization in T cells." PLoS One **8**(12): e82590.

Oppenheimer, D. R. (1978). "The cervical cord in multiple sclerosis." Neuropathol Appl Neurobiol **4**(2): 151-162.

Phillips, M. J., R. O. Weller, S. Kida and F. Iannotti (1995). "Focal brain damage enhances experimental allergic encephalomyelitis in brain and spinal cord." Neuropathol Appl Neurobiol **21**(3): 189-200.

Pines, M., O. Levi, O. Genin, A. Lavy, C. Angelini, V. Allamand and O. Halevy (2017). "Elevated Expression of Moesin in Muscular Dystrophies." Am J Pathol **187**(3): 654-664.

Pore, D. and N. Gupta (2015). "The ezrin-radixin-moesin family of proteins in the regulation of B-cell immune response." Crit Rev Immunol **35**(1): 15-31.

Prineas, J. W. and J. D. Parratt (2012). "Oligodendrocytes and the early multiple sclerosis lesion." Ann Neurol **72**(1): 18-31.

Ruther, B. J., M. Scheld, D. Dreymueller, T. Clarner, E. Kress, L. O. Brandenburg, T. Swartenbroekx, C. Hoornaert, P. Ponsaerts, P. Fallier-Becker, C. Beyer, S. O. Rohr, C. Schmitz, U. Chrzanowski, T. Hochstrasser, S. Nyamoya and M. Kipp (2017). "Combination of cuprizone and experimental autoimmune encephalomyelitis to study inflammatory brain lesion formation and progression." Glia **65**(12): 1900-1913.

Scheld, M., B. J. Ruther, R. Grosse-Veldmann, K. Ohl, K. Tenbrock, D. Dreymuller, P. Fallier-Becker, A. Zendedel, C. Beyer, T. Clarner and M. Kipp (2016). "Neurodegeneration Triggers Peripheral Immune Cell Recruitment into the Forebrain." J Neurosci **36**(4): 1410-1415.

Schwartz-Albiez, R., A. Merling, H. Spring, P. Moller and K. Koretz (1995). "Differential expression of the microspike-associated protein moesin in human tissues." Eur J Cell Biol **67**(3): 189-198.

Sun, D., T. A. Newman, V. H. Perry and R. O. Weller (2004). "Cytokine-induced enhancement of autoimmune inflammation in the brain and spinal cord: implications for multiple sclerosis." Neuropathol Appl Neurobiol **30**(4): 374-384.

Totaro, R., C. Di Carmine, A. Splendiani, S. Torlone, L. Patriarca, C. Carrocci, S. Sciamanna, C. Marini and A. Carolei (2016). "Occurrence and long-term outcome of tumefactive demyelinating lesions in multiple sclerosis." Neurol Sci **37**(7): 1113-1117.

Trepanier, M. O., K. D. Hildebrand, S. D. Nyamoya, S. Amor, R. P. Bazinet and M. Kipp (2018). "Phosphatidylcholine 36:1 concentration decreases along with demyelination in the cuprizone animal model and in post-mortem multiple sclerosis brain tissue." J Neurochem.

van der Valk, P. and C. J. De Groot (2000). "Staging of multiple sclerosis (MS) lesions: pathology of the time frame of MS." Neuropathol Appl Neurobiol **26**(1): 2-10.

van Horssen, J., S. Singh, S. van der Pol, M. Kipp, J. L. Lim, L. Peferoen, W. Gerritsen, E. J. Kooi, M. E. Witte, J. J. Geurts, H. E. de Vries, R. Peferoen-Baert, P. J. van den Elsen, P. van der Valk and S. Amor (2012). "Clusters of activated microglia in normal-appearing white matter show signs of innate immune activation." J Neuroinflammation **9**: 156.

van Noort, J. M., M. Bsibsi, W. H. Gerritsen, P. van der Valk, J. J. Bajramovic, L. Steinman and S. Amor (2010). "Alphab-crystallin is a target for adaptive immune responses and a trigger of innate responses in preactive multiple sclerosis lesions." J Neuropathol Exp Neurol **69**(7): 694-703.

Vitorino, P., S. Yeung, A. Crow, J. Bakke, T. Smyczek, K. West, E. McNamara, J. Eastham-Anderson, S. Gould, S. F. Harris, C. Ndubaku and W. Ye (2015). "MAP4K4 regulates integrin-FERM binding to control endothelial cell motility." Nature **519**(7544): 425-430.